JCB Journal of Cell Biology

ARTICLE

An early endosome–derived retrograde trafficking pathway promotes secretory granule maturation

Cheng-I J. Ma[1,2], Yitong Yang[1,3], Taeah Kim[1,4], Chang Hua Chen[1,4], Gordon Polevoy[1], Miluska Vissa[1,3], Jason Burgess[1,3], and Julie A. Brill[1,2,3]

Regulated secretion is a fundamental cellular process in which biologically active molecules stored in long-lasting secretory granules (SGs) are secreted in response to external stimuli. Many studies have described mechanisms responsible for biogenesis and secretion of SGs, but how SGs mature remains poorly understood. In a genetic screen, we discovered a large number of endolysosomal trafficking genes required for proper SG maturation, indicating that maturation of SGs might occur in a manner similar to lysosome-related organelles (LROs). CD63, a tetraspanin known to decorate LROs, also decorates SG membranes and facilitates SG maturation. Moreover, CD63-mediated SG maturation requires type II phosphatidylinositol 4 kinase (PI4KII)-dependent early endosomal sorting and accumulation of phosphatidylinositol 4-phosphate (PI4P) on SG membranes. In addition, the PI4P effector Past1 is needed for formation of stable PI4KII-containing endosomal tubules associated with this process. Our results reveal that maturation of post-Golgi–derived SGs requires trafficking via the endosomal system, similar to mechanisms employed by LROs.

Introduction

In eukaryotic cells, the secretory pathway is responsible for targeting proteins and lipids to the plasma membrane and the extracellular space. Hence, secretion is essential for cell membrane integrity, cell polarity, and cell-to-cell communication. In conventional secretion, the process is classified into constitutive and regulated secretory pathways. For both pathways, cargo proteins are translated in the ER and trafficked through the Golgi to reach the TGN. At the TGN, cargoes are sorted into secretory vesicles for constitutive secretion or into secretory granules (SGs) for regulated secretion. Unlike constitutive secretion, in which secretory vesicles are rapidly transported to the plasma membrane, cargoes undergoing regulated secretion are stored and processed in SGs that are secreted only on demand.

Professional secretory cells from the endocrine and exocrine systems secrete biologically active molecules through the regulated secretory pathway. In general, cargoes are concentrated at the TGN and bud off as immature SGs, either through aggregation or through the help of various coat and adapter proteins (Asensio et al., 2013; Burgess et al., 2011; Lui-Roberts et al., 2005). Immature SGs then undergo a maturation process through homotypic fusion and remodeling to ensure proper packaging of cargoes and removal of unneeded material (Bonnemaison et al., 2013). Although SGs were initially believed to be solely post-Golgi derived, recent studies suggest that proteins from the endocytic pathway might be required for proper SG biogenesis or function. Endocytic contribution to SG maturation and function has been described in both cultured cell lines and model organisms. In mouse bone marrow–derived mast cells, the early endosome (EE) regulator Rab5 controls SG size and content, whereas Rab27B localizes to SGs and recruits the tetraspanin CD63 from endosomes (Azouz et al., 2014; Klein et al., 2017; Mizuno et al., 2007). In rat pancreatic acinar cells, unwanted content of immature zymogen granules enters the endolysosomal system during remodeling and maturation in a Rab5- and tumor protein D52–dependent manner (Messenger et al., 2013). Dense core vesicles in *Caenorhabditis elegans* neurons require Rab2 and retrograde transport from endosome-associated recycling protein (EARP) complex to mature, and loss of Rab5 or Rab10 activity leads to defects in regulated secretion of dense core vesicles (Ailion et al., 2014; Edwards et al., 2009; Sasidharan et al., 2012; Topalidou et al., 2016). In addition, mucocysts from *Tetrahymena thermophila* need endosomal class C core vacuole/endosome tethering (CORVET) complex subunits for proper maturation (Briguglio et al., 2013; Kontur et al., 2016; Sparvoli et al., 2018).

The larval salivary glands of *Drosophila melanogaster* are a highly accessible genetic model system for studying SG biogenesis (Biyasheva et al., 2001; Burgess et al., 2011, 2012; Torres

[1]Cell Biology Program, The Hospital for Sick Children, Toronto, ON, Canada; [2]Institute of Medical Science, University of Toronto, Toronto, ON, Canada; [3]Department of Molecular Genetics, University of Toronto, Toronto, ON, Canada; [4]Human Biology Program, University of Toronto, Toronto, ON, Canada.

Correspondence to Julie A. Brill: julie.brill@sickkids.ca.

et al., 2014). During early larval development, the salivary gland produces saliva to help moisten food for feeding (Goldstein and Fyrberg, 1994). 24 h after entering the third instar larval stage (L3), the larvae stop feeding and begin production of glue proteins that are packaged into SGs known as glue granules. These SGs mature over the next 18 h and are released in response to a pulse of the hormone ecdysone to stick the pupa onto a solid surface during metamorphosis (Biyasheva et al., 2001; Burgess et al., 2011). Mature SGs are two- to fourfold larger in cross-sectional area than immature SGs, enabling us to employ the fluorescently tagged cargo protein Sgs3-DsRed to visually identify genes required for proper SG maturation. Using this system, we previously demonstrated the importance of type II phosphatidylinositol 4-kinase (PI4KII) in this process. Loss of PI4KII results in failure of SG maturation and defects in late endosome (LE) trafficking, suggesting a potential endocytic contribution to SG maturation via PI4KII activity (Burgess et al., 2012).

PI4KII is one of three PI4Ks in *Drosophila*. PI4Ks phosphorylate PI to form PI 4-phosphate (PI4P), which serves as the precursor to PIP2 and PIP3 and is a crucial signaling molecule on cellular membranes (Tan and Brill, 2014). Unlike the type III PI4Ks, PI4KIIIα and PI4KIIIβ, PI4KII is palmitoylated and inserted in the cytoplasmic leaflet of organelle membranes (Jung et al., 2008). The three PI4Ks produce PI4P on different cellular membranes (Tan and Brill, 2014). PI4KIIIα produces plasma membrane PI4P, whereas PI4KIIIβ (called Four wheel drive [Fwd] in *Drosophila*) synthesizes Golgi PI4P (Polevoy et al., 2009; Tan et al., 2014). PI4KII localizes to the TGN and endosomes, where its catalytic activity is needed for formation of endosomal tubules (Burgess et al., 2012).

In this study, we aimed to discover potential PI4KII mediators involved in SG maturation through a targeted RNAi screen. This screen revealed that post-Golgi–derived SGs require an endocytic contribution to mature. We showed that CD63, an endolysosomal protein that decorates lysosome-related organelles (LROs; Raposo et al., 2007), localizes to the limiting membrane of SGs and regulates SG size. Taking advantage of CD63's ability to promote SG maturation, we performed a secondary screen with CD63 and discovered that PI4KII, Syntaxin 16 (Syx16), and Past1, a PI4P effector (Jović et al., 2009; Koles et al., 2015), act in the same pathway. Moreover, Past1 and Syx16 are essential for PI4KII-mediated endosomal tubulation that is associated with accumulation of PI4P on mature SGs. In summary, we show that Past1, Syx16, and PI4KII support an EE–to–TGN retrograde trafficking pathway that is needed for SG maturation. Our results indicate that SG maturation in the larval salivary gland is surprisingly complex and may share similarity with a subset of LROs.

Results

SG maturation requires endocytic contribution

We previously demonstrated that PI4KII, but not Fwd, is required for SG maturation (Burgess et al., 2012). Because PI4KII and Fwd localize near each other at the TGN and Golgi, we hypothesized that an endosomal defect due to loss of PI4KII might be the underlying cause for failed SG maturation. To identify potential regulators of PI4KII-mediated SG maturation, we screened 254 genes involved in intracellular trafficking, cell polarity, or cytoskeletal dynamics by RNAi (Table S1 A). To induce RNAi, genetically encoded haripin RNAs specific to each gene were expressed in developing salivary gland cells via the galactose metabolism 4/upstream activating sequence (GAL4–UAS) system using the AB1-GAL4 driver (Burgess et al., 2011; Costantino et al., 2008; see Materials and methods). The severity of the effect of gene knockdown on SG biogenesis was scored qualitatively on a scale of 0 to 4 based on the size of the resulting SGs revealed by the fluorescently tagged cargo protein Sgs3-DsRed (Fig. 1 A), where 0 resembled WT controls, 1 showed a slight reduction in SG size, and 4 exhibited severe defects in the production of nascent SGs. Knockdowns resulting in a score of 2 or 3 exhibited SGs that were small enough to be considered as positive hits. More than half (48 of 80) of the positive hits encode proteins involved in endolysosomal trafficking or function (Fig. 1 G). It is possible that this list includes false positives, as we did not verify the specificity of the RNAi lines. However, many of the genes, including those discussed below, were tested with multiple RNAi lines targeting the same gene, showed phenotypes similar to other subunits of the same protein complex, or were verified with null mutants. These include genes encoding the SNAREs Syx16 and Snap29, which localize to both Golgi and endosomal compartments (Csizmadia et al., 2018; Morelli et al., 2014; Xu et al., 2002); the GTPase Rab5, which regulates trafficking at EE; and the ADP-ribosylation factor-like protein Arl1 and the Eps15 homology domain-containing protein 1 (EHD1) orthologue Past1, which are involved in EE–to–TGN retrograde trafficking (Fig. 1, B–F; Christis and Munro, 2012; D'Souza et al., 2014; McKenzie et al., 2012; Sharma et al., 2009). Thus, SG maturation requires endosomal trafficking proteins.

The endosomal tetraspanin CD63 localizes to SG membranes and promotes their maturation

Because of the large contribution of endocytic genes, we hypothesized that SG maturation might employ pathways similar to those involved in LRO maturation. Although most LROs originate from the endolysosomal system, a subset of LROs, namely Weibel-Palade bodies (WPBs), originate from the TGN and acquire endocytic material during maturation (Marks et al., 2013). To investigate whether SGs share similar properties to these LROs, we expressed a well-characterized LRO marker, fluorescently tagged mouse tetraspanin CD63 (CD63-GFP). In contrast to controls lacking CD63-GFP expression, cells expressing one copy of the CD63-GFP transgene had larger SGs, and CD63-GFP localized to the membranes of SGs containing the fluorescent cargo protein Sgs3-DsRed (Fig. 2, A–B′′). In addition, SGs became abnormally large when CD63-GFP was expressed at higher levels using two copies of the transgene (Fig. 2, C–C′′). Quantification of the cross-sectional area of these SGs revealed a positive correlation between CD63-GFP expression level and SG size (Fig. 2 D; see Materials and methods). As CD63-GFP expression levels increased, the distribution of SG size shifted toward SGs >15 μm^2 in cross-sectional area (Fig. 2 E). The ability of CD63-GFP to promote SG maturation was not an artifact of expression of the mammalian protein, as overexpression of the

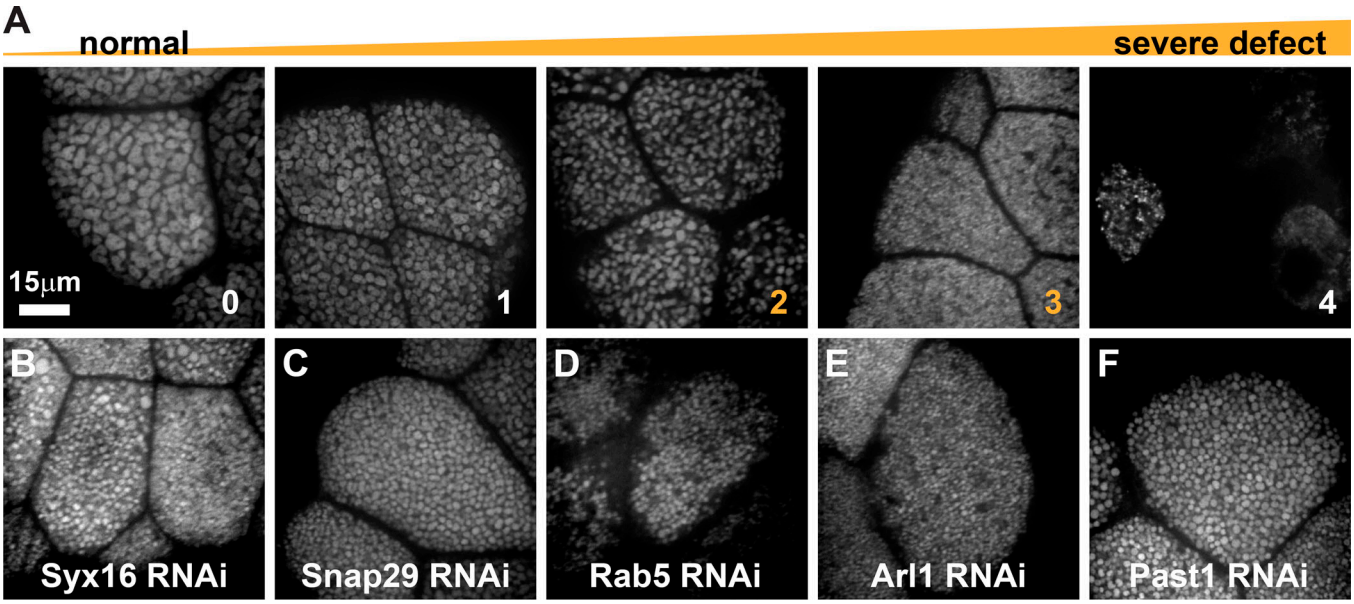

G

Endocytosis	AP-2 (α, σ, μ), Shi, Synj
Early Endosome	Rab5, Rabex5, Rbpn-5, Vha55, Vps34, Vps45
ESCRT-0	Hrs
ESCRT-I	Mvb12
ESCRT-II	Vps22, Vps25, Vps36
ESCRT-III	Vps24, Vps32, CHMP2B
CORVET/HOPS	Vps18, Vps33A, Vps39
LRO-related	Blos1, Dysb, Snapin, HPS1
GARP	Vps 51, Vps52, Vps53, Vps54
Retrograde to TGN	Arl1, Lqfr, Past1, Snx3, Vps13
Recycling Endosome	Rab11
Lysosome	Spinster, Tumor D52
Autophagy	Atg1, Atg5
SNAREs	γSnap, Snap29, Syx7, Syx13, Syx16, Syx17, VAMP7, Vti1a
Tetraspanins	Tsp29Fa, Tsp39D, Tsp42A

Figure 1. **Targeted RNAi screen identifies endosomal genes involved in SG maturation. (A–F)** Spinning-disc confocal images of live L3 salivary gland cells expressing Sgs3-DsRed (grayscale). **(A)** Examples of SG RNAi phenotypes scored on a scale from 0 (normal) to 4 (severe). **(B–F)** Examples of RNAi knockdowns showing defects in SG maturation. **(G)** List of positive hits from the endocytic pathway.

Drosophila CD63 homologue Tsp29Fa also increased SG size (Fig. 2, F–I). To examine whether CD63 and Tsp29Fa act similarly in this process, colocalization of the two proteins was examined by coexpressing and immunostaining CD63-GFP and Tsp29Fa-Flag-HA in early and late L3 salivary glands (Fig. S1, A–B′′). We performed Pearson's correlation coefficient and Mander's overlap coefficient analyses. Pearson's measures the correlation between the fluorescence intensity of two proteins based on their overlapping pixels, and Mander's measures the degree of overlap of one protein with another protein. In early L3 salivary gland cells, Tsp29Fa-Flag-HA distribution correlated with CD63-GFP (Fig. S1 C, Pearson's = 0.43 ± 0.13). In late L3 salivary gland cells, CD63-GFP and Tsp29Fa-Flag-HA showed weaker correlation (Fig. S1 D, Pearson's = 0.22 ± 0.041), but the two proteins exhibited strong cooccurrence on SG membranes (Mander's CD63 = 0.51 ± 0.084, Mander's Tsp29Fa = 0.47 ± 0.14). Moreover, cooverexpression of one copy of Tsp29Fa-HA and one copy of CD63-GFP resulted in abnormally large SGs, similar to overexpressing two copies of CD63-GFP (Fig. S1 E) and further indicating that Tsp29Fa and CD63 share a conserved function.

To determine how CD63-GFP and Tsp29Fa overexpression affects intracellular transport, we examined markers for secretory and endosomal trafficking. To examine secretion, we expressed fluorescently tagged mouse transmembrane glycoprotein CD8-RFP, which is delivered to the apical membrane in control salivary gland cells. When coexpressed, both CD63-GFP and CD8-RFP localized to the apical membrane (Fig. S1 F), indicating that the increase in SG size is not caused by a failure in apical secretion. To investigate endosomal transport, we compared the distribution of the EE protein Hrs in control cells with no Tsp29Fa-Flag-HA expression to cells overexpressing Tsp29Fa-Flag-HA (Fig. S1 G). Tsp29Fa-Flag-HA colocalized with Hrs and shifted Hrs toward the cup-like structure formed by the cis-Golgin Lava lamp (Lva; Fig. S1 G). The

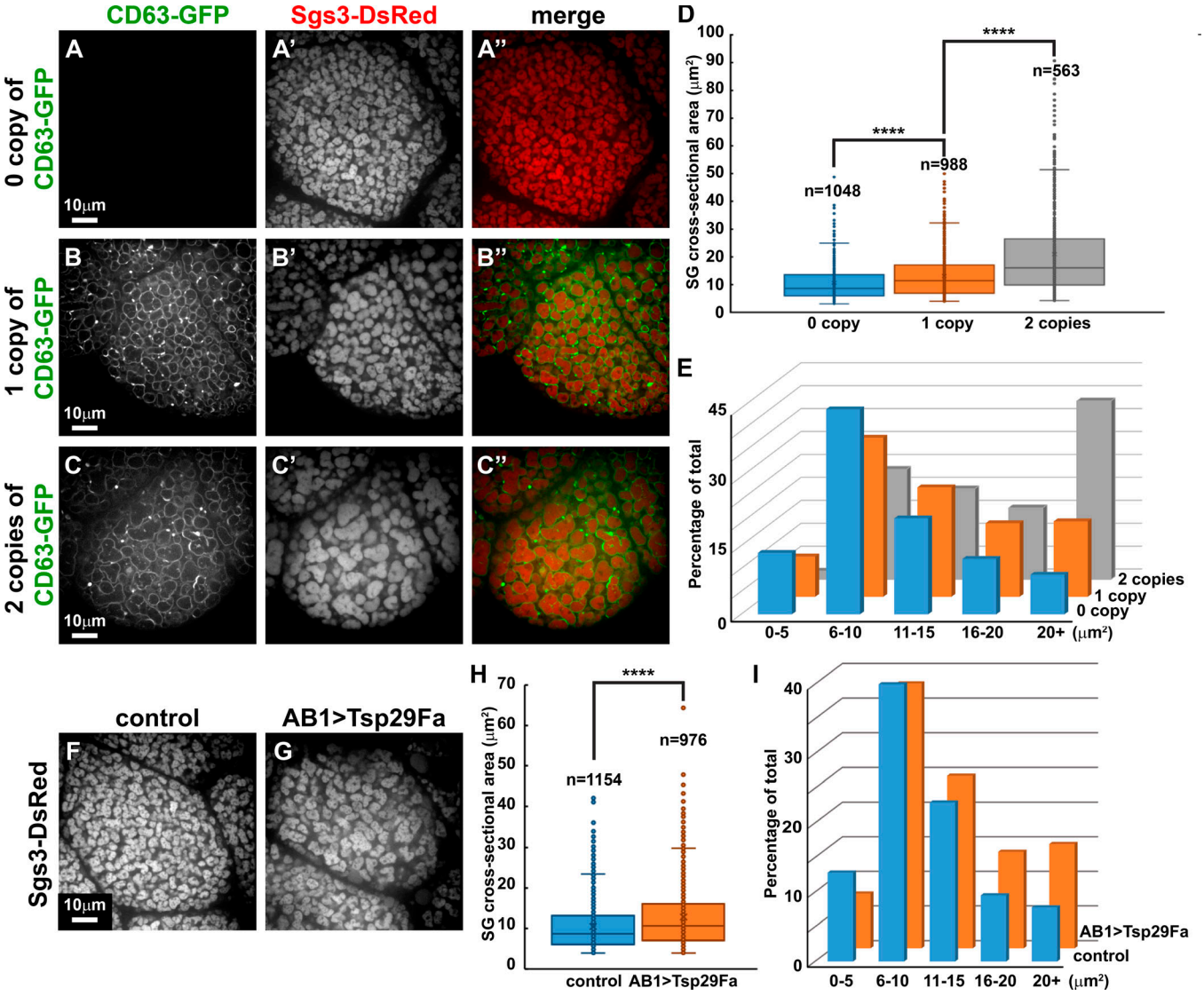

Figure 2. **CD63 and the *Drosophila* homologue Tsp29Fa decorate the limiting membrane of SGs and increase SG size. (A–C, F, G, J, and K)** Spinning-disc confocal images of live L3 salivary gland cells. **(A–C′′)** Cells expressing Sgs3-DsRed (red) with one copy of the AB1-GAL4 driver (A–A′′) or with a single copy of UAS-CD63-GFP (green) driven by a single copy of AB1-GAL4 (B–B′′), or with two copies of UAS-CD63-GFP driven by two copies of AB1-GAL4 (C–C′′). **(D)** Box-and-whisker plot (see Materials and methods) showing the distribution of cross-sectional areas of SGs (from A–C). *n* = total number of SGs in images from three independent salivary glands; ****, P < 0.0001. **(E)** Bar graph showing percentage distribution of SGs with different cross-sectional areas (from A–C). **(F and G)** Cells expressing Sgs3-DsRed (grayscale) with one copy of AB1-GAL4 (F) or two copies of UAS-Tsp29Fa-Flag-HA driven by one copy of AB1-GAL4 (G). **(H)** Box-and-whisker plot (see Materials and methods) showing the distribution of cross-sectional areas of SGs (from F and G). *n* = total number of SGs in images from three independent salivary glands; ****, P < 0.0001. **(I)** Bar graph showing percentage distribution of SGs with different cross-sectional areas (from F and G).

localization of this compartment is reminiscent of the TGN (Burgess et al., 2011), suggesting that Tsp29Fa overexpression might influence EE–to–TGN retrograde trafficking.

Drosophila tetraspanin Tsp29Fa is required for proper SG maturation

To evaluate whether endogenous tetraspanins play a role in SG maturation, we knocked down *Tsp29Fa* expression using RNAi. SGs in *Tsp29Fa* knockdowns were significantly smaller than in controls (Fig. 3, A, B, and G), and expression of CD63-GFP suppressed the *Tsp29Fa* RNAi phenotype (Fig. 3, C and G). To further confirm the role of Tsp29Fa in SG maturation, we generated two deletion mutants using CRISPR-Cas9 gene editing (Fig. S2 A). The first mutant, $Tsp29Fa^{J1a}$, is a predicted null allele of *Tsp29Fa*, and the second mutant, *Df(2L)L7a*, deletes nearly all of the coding sequences of *Tsp29Fa* and the neighboring tetraspanin *Tsp29Fb* (Fig. S2, B and C). Tsp29Fb has weaker alignment score with CD63 compared with Tsp29Fa (CD63 vs. Tsp29Fa E-value = 5.0×10^{-41}; CD63 vs. Tsp29Fb E-value = 5.0×10^{-32}). However, both proteins are highly conserved in their transmembrane domains (Fig. S2, B and C). SGs from $Tsp29Fa^{J1a}$ homozygotes had a mild but significant defect in SG maturation (Fig. 3, D, E, and H), whereas SGs from *Df(2L)L7a* homozygotes were even smaller (Fig. 3, E, F, and H). To address whether *Tsp29Fb* expression is

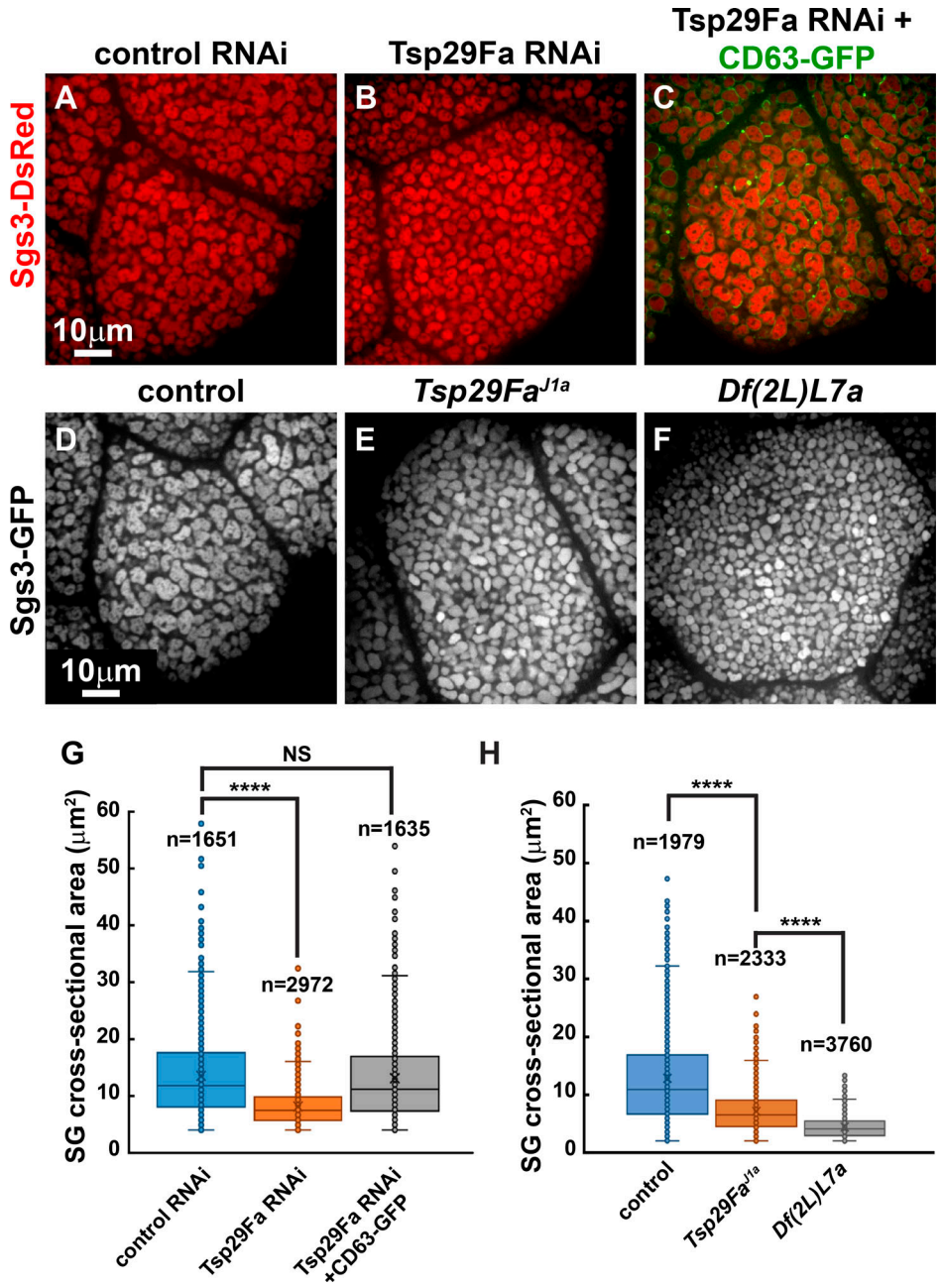

Figure 3. **Tsp29Fa is required for normal SG maturation. (A–F)** Spinning-disc confocal images of live L3 salivary gland cells expressing Sgs3-DsRed (red; A–C) or Sgs3-GFP (grayscale; D–F). **(A–C)** Cells from RNAi control (A), *Tsp29Fa* knockdown (B), or *Tsp29Fa* knockdown expressing CD63-GFP (green, C). **(D–F)** Cells from control (D), *Tsp29*^{J1a} (E), and *Df(2L)L7a* (F). **(G)** Box-and-whisker plot (see Materials and methods) showing the distribution of cross-sectional areas of SGs (from A–C). *n* = total number of SGs in images from three independent salivary glands; ****, P < 0.0001. **(H)** Box-and-whisker plot (see Materials and methods) showing the distribution of cross-sectional areas of SGs (from D–F). *n* = total number of SGs in images from three independent salivary glands; ****, P < 0.0001.

up-regulated in response to loss of *Tsp29Fa*, quantitative PCR was performed on WT and *Tsp29Fa*^{J1a} L3 larvae, and no significant change in *Tsp29Fb* RNA expression level was observed (Fig. S2 D). Thus, CD63 family members share the ability to promote SG maturation.

EE trafficking proteins are necessary for CD63 function

To identify genes required for CD63 function in SG maturation, we expressed CD63-GFP in the background of different RNAi knockdowns from our initial screen (Table S1 B). Expression of CD63-GFP suppressed the knockdown phenotypes of some but not all of the genes (Fig. 4, A–F′). Altogether, 21 of 37 knockdowns tested were suppressed by CD63-GFP (Table S1 B). For example, the knockdown phenotype of clathrin adapter subunit *AP-2σ* was suppressed (Fig. 4, A and A′), and EE regulator *Rab5* appeared to be partially suppressed (Fig. 4, B and B′) by CD63-GFP expression. Notably, expression of CD63-GFP had no effect on SG maturation in the remaining knockdowns tested (16 of 37).

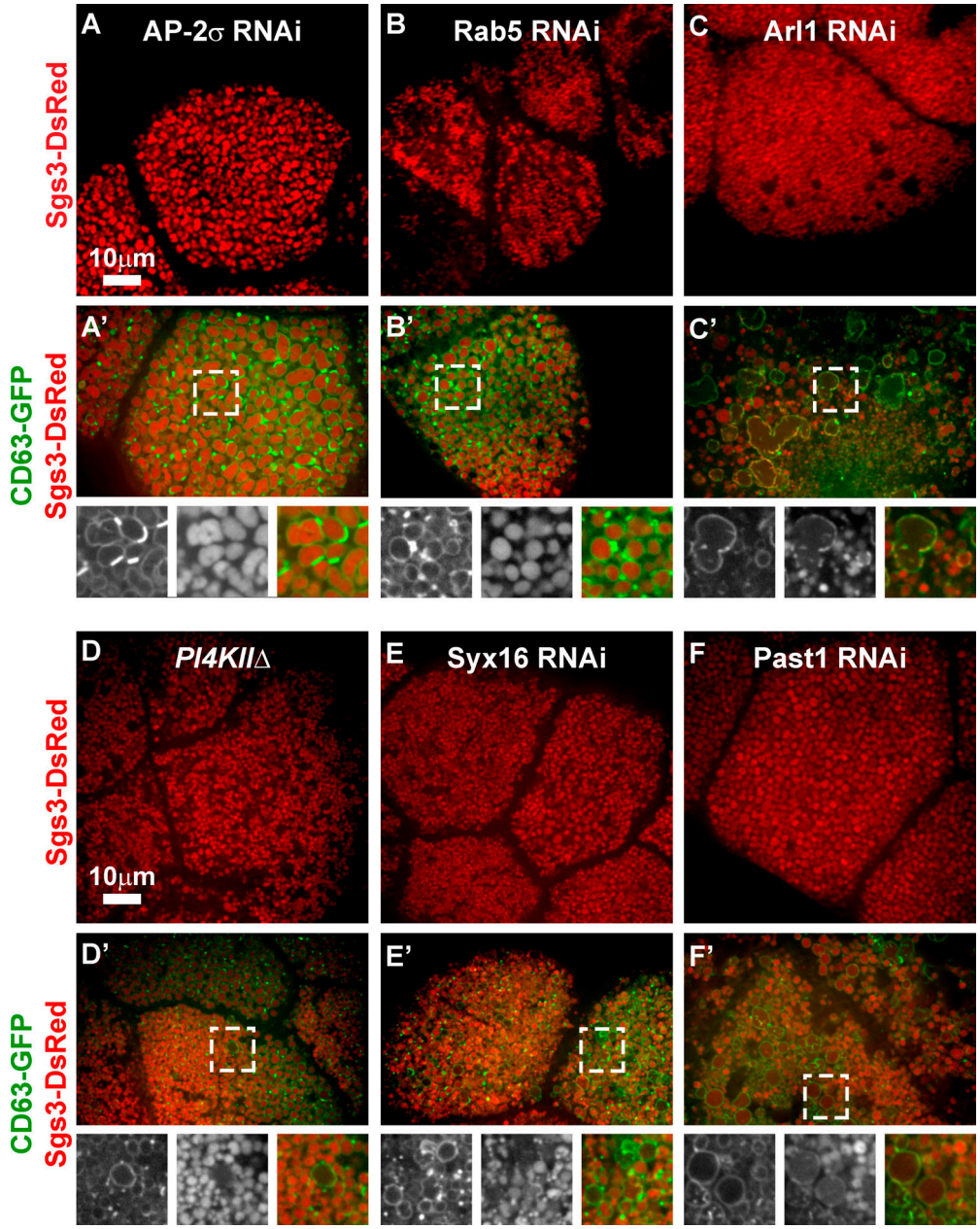

Figure 4. **CD63 requires EE–to–TGN retrograde trafficking to facilitate SG maturation. (A–F′)** Spinning-disc confocal images of live L3 salivary gland cells expressing Sgs3-DsRed (red) in different RNAi backgrounds without (A–F) or with (A′–F′) coexpression of CD63-GFP (green). Dashed boxes mark regions magnified twofold in the insets.

These included genes involved in retrograde trafficking such as *Syx16*, *Past1*, and *Arl1*. Localization of CD63-GFP in knockdowns of *Syx16* and *Past1* (Fig. 4, E–F′) resembled CD63-GFP localization in *PI4KII* null mutants (*PI4KIIΔ*; Fig. 4, D and D′). CD63-GFP remained on small SGs and decorated enlarged endosomes that often contained a faint Sgs3-DsRed signal. This similarity suggested that *Syx16*, *Past1*, and *PI4KII* might act in the same pathway, and that endosome–to–TGN retrograde trafficking might be required for CD63 to promote SG maturation. In contrast to *Syx16*, *Past1*, and *PI4KII*, the defects in knockdowns of *Arl1* were enhanced by CD63-GFP expression, revealing accumulation of CD63 on extremely large (>5-μm–diameter) endosomes (Fig. 4, C and C′). Because many of the nonsuppressible genes act at EEs or in retrograde trafficking, it is likely that retrograde trafficking from EEs, rather than LEs, promotes SG maturation.

PI4KII is important for proper EE dynamics

Based on our genetic analysis, we suspected that PI4KII, Past1, and Syx16 mediate EE–to–TGN retrograde trafficking to promote SG maturation. To investigate whether loss of PI4KII affects EE function, we expressed the PI3P binding EE probe GFP-2xFYVE (Gillooly et al., 2000; Jean et al., 2012; Juhász et al., 2008) in WT and *PI4KIIΔ* salivary glands. In controls, GFP-2xFYVE localized to small and large puncta near SGs marked by Sgs3-DsRed (Fig. 5

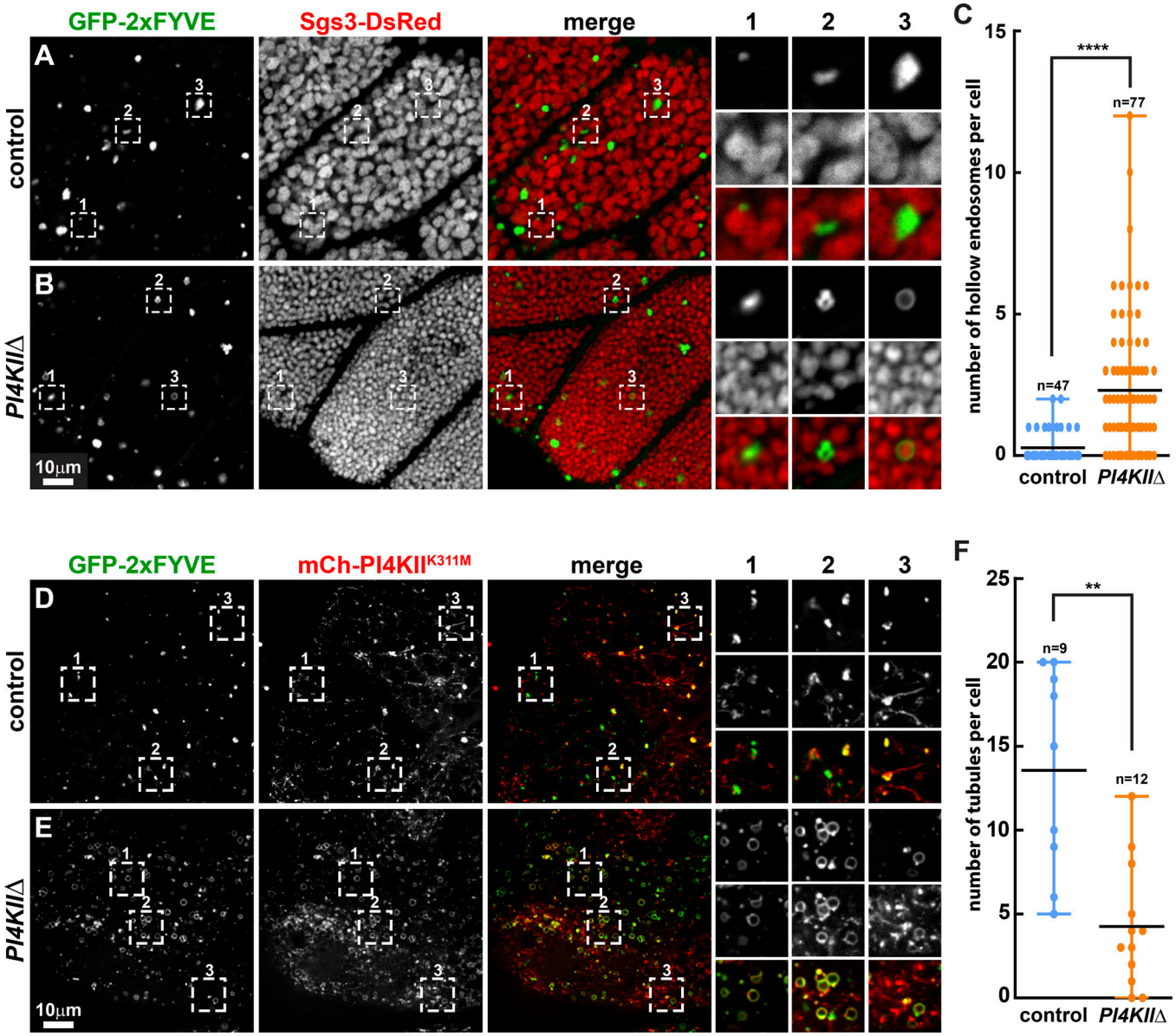

Figure 5. **PI4KII localizes to EEs and modulates EE dynamics. (A and B)** Nikon point-scanning confocal images of live late L3 salivary gland cells expressing GFP-2xFYVE (green) and Sgs3-DsRed (red) in control (A) or *PI4KIIΔ* mutant (B). Dashed boxes mark regions magnified 2.8-fold in insets. **(C)** Plot depicting number of hollow endosomes per cell in control and *PI4KIIΔ* mutant. Top and bottom bars indicate maxima and minima of the datasets. *n* = total number of cells in images from six (control) or 10 (*PI4KIIΔ*) independent salivary glands; ****, $P < 0.0001$. **(D and E)** Spinning-disc confocal images of live L3 salivary gland cells expressing GFP-2xFYVE (green) and mCh-PI4KII^{ATP} (red) in control (D) or *PI4KIIΔ* mutant (E). Dashed boxes mark regions magnified 2.1-fold in insets. **(F)** Plot depicting number of PI4KII tubules per cell in individual optical sections from control and *PI4KIIΔ* mutant. Top and bottom bars indicate maxima and minima of the datasets. Black bar indicates the mean. *n* = total number of cells in images from three independent salivary glands; **, $P < 0.01$.

A). In *PI4KIIΔ*, GFP-2xFYVE marked additional enlarged vesicular structures that were occasionally filled with Sgs3-DsRed (Fig. 5 B). Counting the number of hollow endosomes in WT and *PI4KIIΔ* showed that their occurrence was significantly higher in *PI4KIIΔ* (Fig. 5 C). To test whether PI3P normally accumulates on immature SGs, early L3 salivary glands were examined, and no PI3P was observed on immature SGs of either WT or *PI4KIIΔ* cells (Fig. S3 B). To further evaluate the role of PI4KII at EE, we coexpressed GFP-2xFYVE with a kinase-dead PI4KII tagged with mCherry (mCh-PI4KII^{K311M}; Burgess et al., 2012). In controls, mCh-PI4KII^{K311M} partially colocalized with GFP-2xFYVE on endosomes and decorated tubular structures extending from these endosomes that lacked the GFP-2xFYVE signal (Fig. 5 D). In *PI4KIIΔ*, mCh-PI4KII^{K311M} partially colocalized with GFP-2xFYVE on enlarged endosomes that exhibited significantly fewer and less extensive mCh-PI4KII^{K311M}–positive tubules (Fig. 5, E and F). These observations indicate that PI4KII activity is required for proper EE organization.

PI4P distribution on mature SGs requires PI4KII

To investigate whether trafficking of CD63-GFP occurs via PI4-KII tubules, we coexpressed CD63-GFP and mCh-PI4KII (Fig. 6,

A–A′′; and Fig. S4 A). No correlation was observed between CD63-GFP and mCh-PI4KII (Fig. 6 B, Pearson's = −0.053 ± 0.025). However, some overlap was observed, as mCh-PI4KII tubules occasionally formed contacts with CD63-GFP–positive SG membranes or endosomes (Fig. 6 B, Mander's PI4KII = 0.36 ± 0.11). When we examined the localization of mCh-PI4KII with CD63-GFP in the *PI4KIIΔ* mutant background, it appeared that mCh-PI4KII also localized to SGs and partially decorated SG membranes (Fig. S3 B), raising the possibility that mCh-PI4KII localizes less efficiently to SGs than the endogenous, untagged PI4KII. In contrast, coexpressing kinase-dead mCh-PI4KII^{D465A} with CD63-GFP in the *PI4KIIΔ* mutant background resulted in concentration of mCh-PI4KII^{D465A} signal inside CD63-GFP–positive organelles (Fig. S3 B), suggesting that kinase-dead PI4KII is sorted into multivesicular bodies when CD63-GFP is expressed in the absence of WT PI4KII. CD63-GFP localized to the limiting membranes of small SGs in *PI4KIIΔ* mutants and knockdowns of *Syx16* and *Past1* (Fig. 4, D′, E′, and F′), raising the question of how SGs acquired CD63-GFP if the retrograde trafficking pathway was compromised. We hypothesized that immature SGs would acquire some CD63-GFP as they bud from the TGN, because CD63 is normally secreted to the plasma membrane before entering the endosomal system (Duffield et al., 2003; Pols and Klumperman, 2009; Schulze et al., 2017; Yu et al., 2016). This is likely the case, as we observed CD63-GFP on immature SG membranes in early L3 salivary gland cells from both WT controls and *PI4KIIΔ* mutants (Fig. S3 C).

Because CD63-GFP and mCh-PI4KII showed poor colocalization, we decided to investigate whether the lipid product of PI4KII colocalizes with CD63-GFP. To test this, we expressed CD63-GFP with the pan-PI4P probe mCh-2xP4M (see Materials and methods; Hammond et al., 2014) in WT salivary gland cells. Both markers localized to SG membranes and endosomes with good correlation (Fig. 6, C and D; and Fig. S4 A, Pearson's = 0.41 ± 0.067). In contrast, distribution of GFP-PI4KII and mCh-2xP4M showed a weaker correlation, but PI4KII overlapped significantly with mCh-2xP4M (Fig. 6, E and F; and Fig. S4 A, Pearson's = 0.32 ± 0.085, Mander's PI4KII = 0.90 ± 0.036, Mander's 2xP4M = 0.36 ± 0.050). The lower overlap of 2xP4M with PI4KII was expected, because P4M labels cellular PI4P ubiquitously and is not restricted to PI4P synthesized by PI4KII. To determine whether PI4P distribution on SG membranes depends on PI4KII activity, we coexpressed Sgs3-GFP with mCh-2xP4M in WT and *PI4KIIΔ* salivary gland cells. In control cells, mCh-2xP4M decorated most of the SGs marked by Sgs3-GFP (Fig. 6, G–G′′), whereas in *PI4KIIΔ* cells, the number of mCh-2xP4M–positive SGs was significantly reduced (Fig. 6, H and I; and Fig. S4 B). Hence, mCh-2xP4M colocalizes strongly with CD63-GFP on SG membranes, and this association requires PI4KII.

Past1 regulates PI4KII tubulation and PI4P accumulation on SG membranes

Our CD63-GFP secondary screen results suggested that *Past1* and *Syx16* might act in the same pathway as *PI4KII* to promote SG maturation. Past1 is important for the initiation and dynamics of EE membrane tubules and is a potential PI4P-binding protein (Jović et al., 2009; Koles et al., 2015). Thus, we evaluated the effect of a *Past1* null mutant (*Past1$^{110-1}$*) on PI4KII tubule formation. Tubules marked by GFP-PI4KII were less extensive in *Past1$^{110-1}$* salivary gland cells, and GFP-PI4KII decorated abundant enlarged organelles that were absent in controls (Fig. 7, A and B; and Fig. S4 C). Knockdown of *Syx16* caused a similar phenotype (Fig. 7 C and Fig. S4 C). To examine whether loss of Past1 also affected the dynamics of PI4KII-positive tubules, we performed live imaging of GFP-PI4KII in control and *Past1$^{110-1}$* salivary glands (Video 1). These experiments revealed that GFP-PI4KII tubules in *Past1$^{110-1}$* extended and retracted significantly faster than in controls (Fig. 7, D–F; *, P = 0.002). To assess whether loss of Past1 compromised PI4KII-mediated retrograde trafficking that is important for SG maturation, we examined changes in PI4P distribution in *Past1$^{110-1}$* salivary gland cells. Localization of mCh-2xP4M to SGs was reduced in *Past1$^{110-1}$* mutants (Fig. 7, G–H′′; and Fig. S4 D), similar to *PI4KIIΔ* mutants. In addition, mCh-2xP4M accumulated on endosomes in *Past1$^{110-1}$* mutants, but only rarely in *PI4KIIΔ* mutants (compare Fig. 7, G–H′′ with Fig. 6, G–H′′). Thus, Past1 (and likely Syx16) is required for the abundance and stability of PI4KII tubules that contribute to accumulation of PI4P on mature SGs, which, in turn, is important for CD63 to promote SG maturation.

Discussion

Regulated SGs are thought to mature, in part, through homotypic fusion (Farkaš and Šutáková, 1998; Burgess et al., 2011), yet how this maturation is regulated has remained poorly understood. In this study, we provide evidence that post-Golgi–derived immature SGs require input from the endocytic pathway to fully mature. In particular, we establish that retrograde transport from EEs via PI4KII, Past1, and Syx16 is important for CD63-mediated SG maturation (Fig. 8 A). PI4KII is required for normal EE–TGN retrograde trafficking, and loss of PI4KII results in small SGs and enlarged EEs that contain mistrafficked Sgs3 cargo proteins. Also, loss of PI4KII leads to reduced levels of PI4P on both SG and EE membranes (Fig. 8 B). Past1 and Syx16 are needed for PI4KII activity in retrograde trafficking, which leads to similar phenotypes for SGs and EEs. However, PI4KII remains active in the EEs and increases PI4P levels at EEs (Fig. 8 C).

Because we observed defects in both SG maturation and LE dynamics in *PI4KIIΔ* mutants (Burgess et al., 2012), we included a large number of endosomal genes in our initial RNAi screen to identify genes that might act in the same pathway as *PI4KII*. Many of the positive hits are involved in EE sorting, EE–LE transition, or retrograde trafficking, whereas most of the LE genes tested were negative. The lack of positive LE hits suggests that EE sorting is more important to SG maturation than LE-dependent transport. Moreover, not all retrograde trafficking pathways are critical for SG maturation. For example, none of the retromer or AP-3 subunits tested was required for SG maturation, consistent with our previous observation that these were dispensable for the formation of PI4KII tubules (Burgess et al., 2012).

CD63 was originally named granulophysin and is found on various types of SGs in human tissues (Hatskelzon et al., 1993;

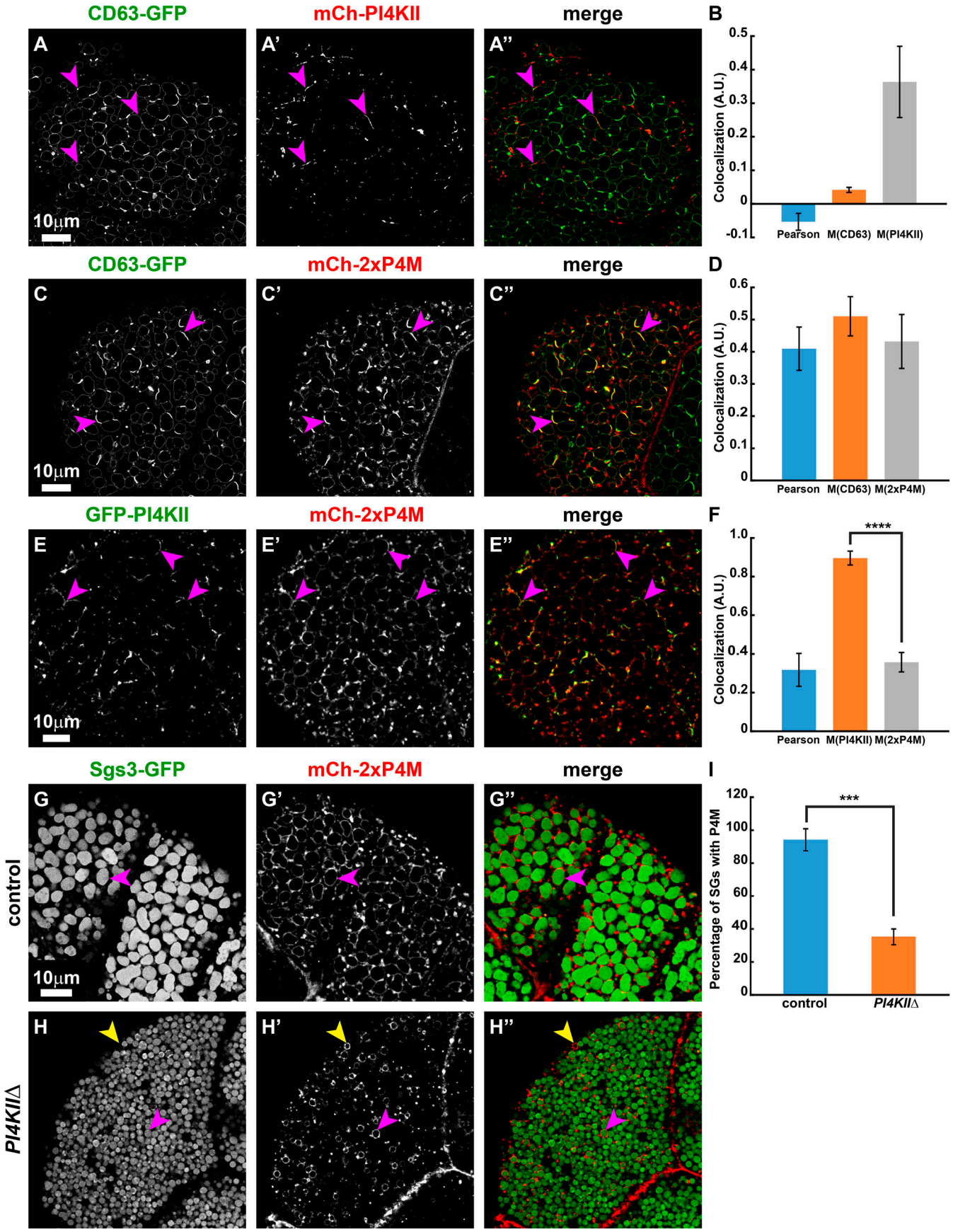
CD63-GFP
mCh-PI4KII
merge
A
A'
A''
10μm
B
Colocalization (A.U.)
0.5
0.4
0.3
0.2
0.1
0
-0.1
Pearson
M(CD63)
M(PI4KII)
CD63-GFP
mCh-2xP4M
merge
C
C'
C''
10μm
D
Colocalization (A.U.)
0.6
0.5
0.4
0.3
0.2
0.1
0
Pearson
M(CD63)
M(2xP4M)
GFP-PI4KII
mCh-2xP4M
merge
E
E'
E''
10μm
F
****
Colocalization (A.U.)
1.0
0.8
0.6
0.4
0.2
0
Pearson
M(PI4KII)
M(2xP4M)
Sgs3-GFP
mCh-2xP4M
merge
control
G
G'
G''
10μm
I
***
Percentage of SGs with P4M
120
100
80
60
40
20
0
control
PI4KIIΔ
PI4KIIΔ
H
H'
H''

Figure 6. **PI4KII is required for accumulation of PI4P on membranes of mature SGs. (A, C, E, G, and H)** Leica point-scanning confocal images of live late L3 salivary gland cells processed with Leica Lightning algorithm. **(A–A′′)** Control cells expressing CD63-GFP (green) and mCh-PI4KII (red). Contacts formed by mCh-PI4KII tubules and CD63-GFP–positive SG membranes are marked by magenta arrowheads. **(B)** Colocalization analysis of CD63-GFP and mCh-PI4KII. Pearson's correlation coefficient = −0.053 ± 0.025, M(CD63) (Mander's overlap coefficient of CD63-GFP) = 0.042 ± 0.0075, M(PI4KII) = 0.36 ± 0.11. Error bars indicate standard deviation. **(C–C′′)** Control cells expressing CD63-GFP (green) and mCh-2xP4M (red). Strong colocalization of CD63-GFP and mCh-2xP4M (yellow) is marked by magenta arrowheads. **(D)** Colocalization analysis of CD63-GFP and mCh-2xP4M. Pearson's = 0.41 ± 0.067, M(CD63) = 0.51 ± 0.061, M(2xP4M) = 0.43 ± 0.084. Error bars indicate standard deviation. **(E–E′′)** Control cells expressing GFP-PI4KII (green) and mCh-2xP4M (red). Colocalization of GFP-PI4KII and mCh-2xP4M on SG membranes is marked by magenta arrowheads. **(F)** Colocalization analysis of GFP-PI4KII and mCh-2xP4M. Pearson's = 0.32 ± 0.085, M(PI4KII) = 0.90 ± 0.036, M(2xP4M) = 0.36 ± 0.050; ****, P < 0.0001. Error bars indicate standard deviation. **(G and H)** Cells expressing Sgs3-GFP (green) and mCh-2xP4M (red) in control (G) or *PI4KIIΔ* mutant (H). SGs coated by mCh-2xP4M are marked by magenta arrowheads. mCh-2xP4M vesicle lacking Sgs3-GFP is marked by yellow arrowhead. **(I)** Percentage of SGs coated by mCh-2xP4M. *n* = one cell each from three independent salivary glands; ***, P < 0.001. Error bars indicate standard deviation.

Nishibori et al., 1993). However, it was unclear whether CD63 plays a functional role in the biogenesis of these SGs or simply decorates SG membranes. Our results identify a positive correlation between CD63 expression level and SG size. This correlation is not a result of compromised exocytosis, as transport of CD8 to the apical membrane is unaffected by CD63 expression. CD63 and *Drosophila* Tsp29Fa are functionally conserved; they localize to SG membranes and act synergistically to promote SG maturation. Although Tsp29Fa and CD63 overlap in their distribution on SG membranes, their correlation is relatively weak, suggesting they might localize to different subdomains. Interestingly, overexpression of Tsp29Fa results in increased localization of EEs in proximity to the TGN, suggesting that overexpression of Tsp29Fa and CD63 may alter EE sorting and trafficking in a manner that facilitates retrograde transport to the Golgi. Indeed, it is possible that overexpression of CD63 promotes SG maturation by up-regulating the retrograde trafficking pathway. Although it remains uncertain how CD63 acts in this process, our results demonstrate that CD63 not only decorates SG membranes but also plays a functional role in SG maturation.

Loss of *Tsp29Fa* does not affect SG maturation to the same extent as in *PI4KIIΔ* or *Pastl*$^{110\text{-}1}$ mutants. The defect in SG maturation is stronger when both *Tsp29Fa* and *Tsp29Fb* are deleted in the *Df(2L)L7a* mutant. This suggests that *Tsp29Fa* and *Tsp29Fb* may be partially redundant. Because tetraspanins can associate to form membrane microdomains (Perez-Hernandez et al., 2013; Verweij et al., 2011), it is likely that that loss of a single tetraspanin could be compensated for by repurposing other tetraspanins. Thus, most animal models of tetraspanin deficiency exhibit relatively mild phenotypes (Geisert et al., 2002; Knobeloch et al., 2000; Maecker and Levy, 1997; Miyazaki et al., 1997; Tarrant et al., 2002). For example, even though CD63 is well characterized for it is importance in melanosome biogenesis, CD63-deficient mice show pronounced pigmentation defects only in retinal pigment epithelia and not other tissues (van Niel et al., 2011). Moreover, *Drosophila* has other putative CD63 homologues, namely Tsp39D and Tsp47F. Unlike *Tsp29Fa* and *Tsp29Fb*, which are highly expressed in the gut and salivary gland, *Tsp39D* is highly expressed in the central nervous system, and *Tsp47F* is expressed at very low levels in the adult head. *Tsp39D* knockdown resulted in small SGs, yet this phenotype is not fully suppressed by expression of CD63-GFP, indicating that the role of *Tsp39D* in SG maturation is distinct from *Tsp29Fa*. On the other hand, *Tsp39D* expression is crucial for maintenance of synaptic vesicles in *Drosophila* photoreceptor cells (Tsai et al., 2019), suggesting that CD63 homologues might carry out analogous functions in regulated secretion in different tissues.

Expression of CD63-GFP in RNAi knockdowns that lead to a small granule phenotype provides a sensitive system to identify pathways required for CD63/Tsp29Fa-mediated SG maturation. Suppression of the small granule phenotype could be due to the ability of CD63 to stimulate trafficking through a pathway that is only partially compromised by the RNAi knockdown or to entirely bypass the function of the target gene. For example, CD63 has been reported to increase endocytic flux of H^+/K^+-ATPase in Cos-7 cells and promotes hemocyte-mediated phagocytosis in clams (Duffield et al., 2003; Yu et al., 2016). Thus, CD63-GFP expression may suppress the *AP-2σ* RNAi phenotype by restoring endocytic flux that is important for proper SG maturation. On the other hand, failure of CD63-GFP expression to suppress the RNAi phenotype indicates that the pathway being altered is necessary for CD63-mediated SG maturation. RNAi knockdowns of many EE genes exhibited either weak or no suppression by CD63-GFP, revealing that proper EE sorting is critical for CD63-mediated SG maturation. Moreover, CD63-GFP expression failed to suppress knockdowns of many retrograde trafficking genes, suggesting it is likely that normal EE–to–TGN retrograde trafficking is important for proper SG maturation. Expression of CD63-GFP in the background of *Syx16* and *Pastl* knockdowns resembled CD63-GFP expression in *PI4KIIΔ* mutants. CD63-GFP decorated enlarged endosomes that occasionally contained faint Sgs3-DsRed signal. The faint signal could be a result of impairment in endosomal degradation or expansion of organelle volume. Interestingly, expression of CD63-GFP in the knockdowns of *Arl1* and subunits of Golgi-associated retrograde protein complex (GARP) resulted in abnormally large endosomes. It is possible that knockdowns of *Arl1* and GARP complex subunits result in blockade of multiple retrograde trafficking pathways and that expression of CD63 leads to fusion of the resulting enlarged endosomes.

Prior biochemical studies have suggested that CD63 and PI4KII may act in concert. PI4KII activity is present in immunoprecipitates of CD63 from human cultured cells (Berditchevski et al., 1997; Yauch and Hemler, 2000). Nonetheless, the physiological consequences of this interaction have remained unclear. Although we were unsuccessful at coimmunoprecipitating CD63 with PI4KII (not depicted) and we did not directly observe CD63 on PI4KII-positive tubules, our data provide evidence that CD63 requires PI4KII activity to promote SG

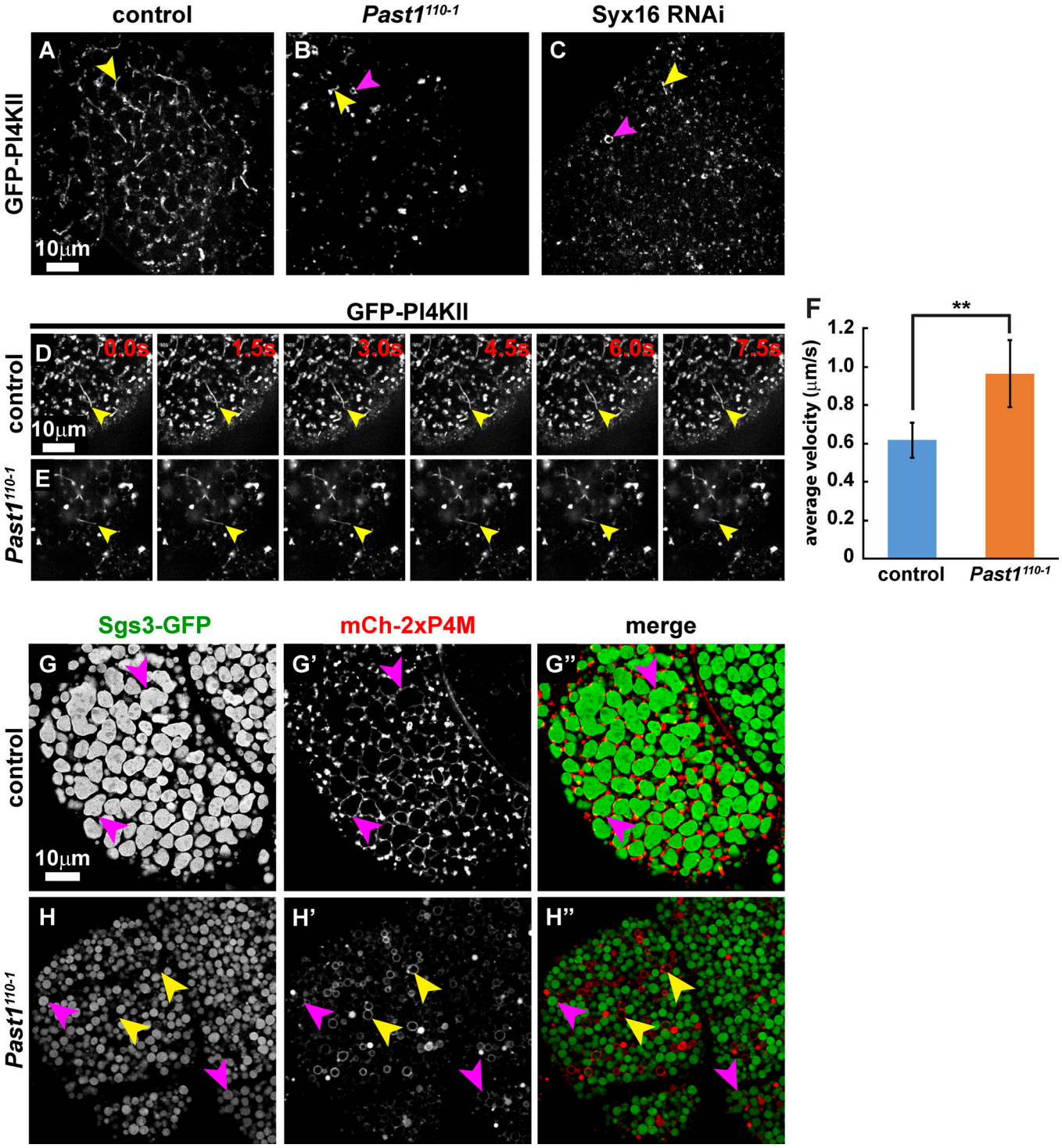

Figure 7. **Past1 and Syx16 control PI4KII tubulation and PI4P accumulation on SG membranes. (A–E)** Spinning-disc confocal images of live L3 salivary gland cells. GFP-PI4KII (grayscale) localization in control (A), *Past1*$^{110\text{-}1}$ (B), and *Syx16* RNAi (C) salivary gland cells. GFP-PI4KII tubules are marked by yellow arrowheads. **(D and E)** Still images of GFP-PI4KII tubule dynamics tracked by yellow arrowheads in control (D) and *Past1*$^{110\text{-}1}$ mutant (E). See Video 1 for the original videos. **(F)** Average velocity of the tips of GFP-PI4KII tubules in control and *Past1*$^{110\text{-}1}$ mutant. *n* = total of five tubules from two independent salivary glands per genotype; **, P < 0.01. Error bars indicate standard deviation. **(G and H)** Leica point-scanning confocal images of live late L3 salivary gland cells processed with Leica Lightning algorithms. Cells expressing Sgs3-GFP (green) and mCh-2xP4M (red) in control (G) or *Past1*$^{110\text{-}1}$ mutant (H) SGs coated by mCh-2xP4M are marked by magenta arrowheads. mCh2-xP4M endosome lacking Sgs3-GFP is marked by yellow arrowhead.

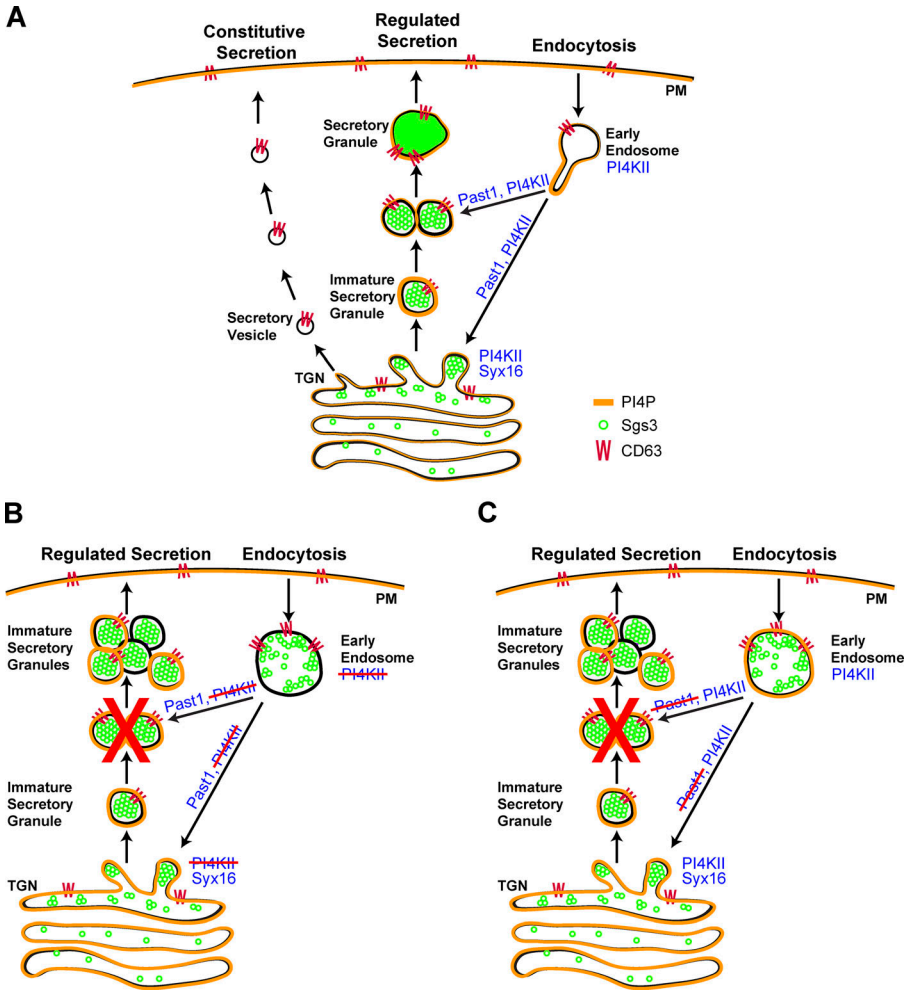

Figure 8. **Working model. (A)** In WT salivary gland cells, EE–TGN retrograde trafficking mediated by Past1, PI4KII, and Syx16 is required for normal SG maturation. PI4P is observed on both EEs and SGs. CD63 also reaches apical membrane through constitutive secretion. **(B)** Loss of PI4KII results in formation of enlarged EEs, lack of endosomal tubules, and failure of SG maturation. PI4P also fails to accumulate on SG membranes due to the loss of PI4KII-mediated retrograde trafficking. **(C)** Loss of Past1 or knockdown of Syx16 results in formation of enlarged EEs and failure of SG maturation due to defects in PI4KII-dependent endosomal tubule formation and retrograde trafficking. As a result, PI4P levels on SGs are reduced and PI4P accumulates on EEs.

maturation. For example, PI4KII tubules formed contacts with CD63-positive SG membranes in WT salivary glands. Moreover, mCh-PI4KII decorated SG membranes together with CD63-GFP when coexpressed in *PI4KIIΔ* mutants. It is possible that mCh-PI4KII weakly localizes to SG membranes and that this is more apparent in the absence of endogenous PI4KII. Furthermore, strong colocalization was observed between CD63 and PI4P, the enzymatic product of PI4KII, on SG membranes. Generation of PI4P on SG membranes was strongly dependent on PI4KII activity, as loss of PI4KII significantly reduced the number of PI4P-positive SGs. In mammalian systems, PI4KII has been reported to associate with SGs, but it is unknown whether PI4KII synthesizes PI4P on SG membranes (Guo et al., 2003; Kristiansen et al., 1998; Panaretou and Tooze, 2002; Del Vecchio and Pilch, 1991; Xu et al., 2006). Moreover, the role of PI4P on SG membranes is unclear. One possibility is that proper levels of PI4P might be required for recruitment of PI4P-binding adapter proteins to facilitate remodeling of SGs during maturation (Mills et al., 2003; Wang et al., 2007, 2003). Another possibility is that CD63 requires PI4P to promote SG maturation.

We demonstrate that Past1 and Syx16 are responsible for the formation and stability of PI4KII-positive tubules. Loss of PI4KII-positive tubules results in an accumulation of PI4P on endosomes, reduction of PI4P on SGs, and failure of SG maturation. Mammalian EHD proteins are associated with endosomal tubulation and PI4P binding (Jović et al., 2009). However, it was initially unclear whether these proteins tubulate membranes, stabilize membrane tubules, or promote tubule vesiculation (Sharma et al., 2009). Indeed, EHD1 is needed for tubule vesiculation, whereas the related family member EHD3 promotes membrane tubulation and tubule stabilization (Bahl et al., 2016; Cai et al., 2013). In terms of sequence homology, *Drosophila* Past1 is more similar to human EHD1 (Gramates et al., 2017). However, the requirement for Past1 in tubulation and stabilization of PI4KII-positive endosomal tubules reveals functional similarity to EHD3, at least in the context of the larval salivary gland.

PI4KII orthologues were recently shown to be required for the maturation of WPBs, which, like large dense core vesicles, are post-Golgi–derived granules that are often considered as part of the LRO family because they require endocytic trafficking during their biogenesis. However, although AP-3 is required for targeting CD63 to mature WPBs and large dense core vesicles (Grabner et al., 2006; Harrison-Lavoie et al., 2006), AP-3 is dispensable for glue granule maturation (Burgess et al., 2012; this study). Nevertheless, the requirement for CD63- and PI4KII-dependent retrograde trafficking indicates that glue granules are

among a subset of SGs that require endosomal trafficking (Ailion et al., 2014; Azouz et al., 2014; Cattin-Ortolá et al., 2017; Klein et al., 2017; Sparvoli et al., 2018; Topalidou et al., 2016).

In conclusion, our work provides additional evidence that SG maturation is not isolated in the post-Golgi compartment and requires endocytic contribution. We demonstrate that Past1 and Syx16 regulate PI4KII-mediated retrograde transport that is critical for CD63 to promote SG maturation. It will be of interest to determine if endocytic contribution is a general feature of SG maturation. Importantly, defects in SG maturation could result in improper packaging of cargoes such as hormones, neurotransmitters, and mucins that may lead to physiological disorders. Therefore, unraveling mechanisms required for SG maturation could provide novel therapeutic insight into diseases associated with SG dysfunction.

Materials and methods

Fly genetics

Flies were cultured on standard cornmeal molasses agar at 25°C (Ashburner, 1989). RNAi stocks expressing hairpin RNAs directed against individual genes were acquired from Bloomington Drosophila Stock Center (BDSC) or Vienna Drosophila RNAi Center (VDRC) as noted (Table S1). Additional stocks included *P{GawB}AB1-GAL4* (BDSC); *P{w+, CG14671}*, *P{neoFRT}82B*, *Df(3R)730* (PI4KIIΔ; Burgess et al., 2012); w^{1118};;$Past1^{110\text{-}1}$ (Olswang-Kutz et al., 2009; a gift from M. Horowitz, Tel Aviv University, Tel Aviv, Israel); *P{w+, UAS-CD63-EGFP}* (Corrigan et al., 2014; Panáková et al., 2005; Redhai et al., 2016; a gift from C. Wilson, University of Oxford, Oxford, UK); *P{w+, UAS-GFP-myc-2xFYVE}* (BDSC); *P{w+, UAS-mCherry-myc-2xFYVE}* (Jean et al., 2012; a gift from A. Kiger, University of California San Diego, San Diego, CA); *P{w+, Sgs3-DsRed}* (Costantino et al., 2008); *P{w+, Sgs3-GFP}* (Biyasheva et al., 2001); *P{w+, UAS-CD8-EGFP}* (BDSC); *P{w+, UAS-CD8-RFP}* (BDSC); and all of the PI4KII transgenic stocks were previously described. *P{w+, αTub84B-GFP-PI4KII}*; *P{w+, αTub84B-mCh-PI4KII}*; *P{w+, αTub84B-mCh-PI4KII^{ATP}}*; and *P{w+, αTub84B-mCh-PI4KII^{CAT}}* transgenic lines were previously described (Burgess et al., 2012). Note that mCh-PI4KII^{K311M} (ATP-binding mutant) and mCh-PI4KII^{D465A} (catalytic site mutant) were previously designated mChPI4KII^{ATP} and mCh-PI4KII^{CAT}. Both mutations result in a catalytically inactive (kinase-dead) PI4KII enzyme in vitro and behave similarly in rescue experiments (Burgess et al., 2012). *P{w+, Sgs3-DsRed}* was recombined with *P{w+, UAS-CD63-EGFP}* for CD63 coexpression experiments. UAS lines were expressed in salivary gland cells under control of the AB1-GAL4 driver (*P{GawB}AB1*; BDSC).

Molecular biology

For the *Tsp29Fa* target sequence (5′-GGAGTTGGCGCCGTCTATAC[GGG]-3′), the forward gRNA was 5′-CTTCGGAGTTGGCGCCGTCTATAC-3′, and the reverse was 5′-AAACGTATAGACGGCGCCAACTCC-3′. For the *Tsp29Fb* target sequence (5′-GCAGTTGGATAACGGAGAGC[AGG]-3′), the forward gRNA was 5′-CTTCGCAGTTGGATAACGGAGAGC-3′, and the reverse was 5′-AAACGCTCTCCGTTATCCAACTGC-3′. gRNA oligonucleotides from Thermo Fisher Scientific were annealed and subcloned into pU6-BbsI-chiRNA (Addgene plasmid #45946).

Individual CRISPR-Cas9 lines were genotyped using primers flanking *Tsp29Fa* and *Tsp29Fb*. The *Tsp29Fa* forward primer sequence was 5′-GTGAAGTATACGCTTTTCGG-3′, and the reverse was 5′-CGGATTTTAATCTCACGTGC-3′. The *Tsp29Fb* forward primer sequence was 5′-CGCCAAGTACATGCTCATC-3′, and the reverse was 5′-GTGTAGGTGTAGGGTTCGTG-3′. Primers were synthesized by Thermo Fisher Scientific.

P4M is the PI4P-binding domain of the *Legionella* protein SidM (Hammond et al., 2014). 2xP4M sequences were PCR-amplified from a mammalian vector containing GFP-2xP4M (Addgene plasmid #51472) and subcloned into a modified pCaSpeR4 vector containing the *αTub84B* promoter (Marois et al., 2006) and mCherry. The forward primer sequence was 5′-GCTCTAGAAATTCTGGTGGTAGTGCTTC-3′, and the reverse was 5′-GCTCTAGAGCATTCATTTTATGTTTCAGG-3′. Primers were synthesized by Thermo Fisher Scientific.

RNA isolation and quantitative real-time PCR (qRT-PCR) of late L3 larvae

RNA was extracted from 10 w^{1118} and $Tsp29Fa^{J1a}$ late L3 larvae using PureLink RNA Mini Kit (Thermo Fisher Scientific). cDNA library was generated using SensiFAST cDNA Synthesis Kit (Bioline). qRT-PCR was performed using PowerUp SYBR Green Master Mix (Thermo Fisher Scientific) on a ViiA 7 Real-Time PCR System (Thermo Fisher Scientific). Forward primer for *α-tubulin* at 84B was 5′-TGTCGCGTGTGAAACACTTC-3′. Reverse primer for *α-tubulin* at 84B was 5′-AGCAGGCGTTTCCAATCTG-3′ (Ponton et al., 2011). *Tsp29Fa* and *Tsp29Fb* primer sequences were obtained from FlyPrimerBank (Harvard Medical School, Cambridge, MA). Primers for *Tsp29Fa* were forward, 5′-AGCGCCAATGCTGTGAAGTAT-3′, and reverse, 5′-GCTTATAGCCCGTATAGACGGC-3′. Primers for *Tsp29Fb* were forward, 5′-CCATCGGATTCATTCTGATCGC-3′, and reverse, 5′-AAGGCACACTCCGTACAGATT-3′. Primers were synthesized by Thermo Fisher Scientific.

Generation of mutants and transgenic flies

pU6 vectors containing gRNAs targeting *Tsp29Fa* and *Tsp29Fb* (Fig. S2) were injected into Cas9-expressing embryos (*PBac{vas-Cas9}VK00027*, BDSC #51324). Injections were done by BestGene. Individual fly lines were screened by PCR for deletions in *Tsp29Fa* and *Tsp29Fb*. UAS-Tsp29Fa-FLAG-HA lines were generated by injecting the UFO04029 plasmid (Drosophila Genomics Resource Center) into embryos containing attP sites (*PBac{y+-attP-3B}VK00002*, BDSC #9723; and *PBac{y+-attP-9A}VK00027*, BDSC #9744) for phiC31 integrase-mediated transgenesis. Injections were done by BestGene. mCh-2xP4M lines were generated by P-element transformation, where the plasmid containing *αTub84B-mCh-2xP4M* was injected into w^{1118} embryos. Injections were done by BestGene.

Microscopy

For live imaging, salivary glands were dissected from early or late L3 larva in 50 µl *Drosophila* Ringer's solution (10 mM Tris, 182 mM KCl, 46 mM NaCl, and 3 mM $CaCl_2 \cdot 2H_2O$, pH 7.2) using fine forceps. Dissected salivary glands were transferred to 30 µl *Drosophila* Ringer's on a microscope slide and sealed using a

coverslip edged with high-vacuum M grease (Apiezon). Samples were imaged using a Quorum spinning-disc confocal coupled with an Olympus IX81 microscope (Quorum Technologies), a Nikon A1R point scanning confocal microscope, or a Leica SP8 Lightning confocal microscope. Images were acquired from the spinning-disc confocal using a 60× oil objective (NA 1.4), a Hamamatsu C9100-13 electron multiplying charge-coupled device camera, and Volocity 6.3 software (PerkinElmer). Serial optical sections were acquired at an interval of 0.3 µm for a total of 20–30 µm. Images acquired from Nikon A1R used a 60× oil objective (NA 1.4) and NIS-Elements software (Nikon). Images acquired from Leica SP8 Lightning confocal used a 40× oil objective (NA 1.3) and LAS-X software (Leica). Leica SP8 images were processed with Lightning using adaptive strategy from the LAS-X software. All images were adjusted for brightness and contrast using Adobe Photoshop CS6.

Immunofluorescence

Salivary glands were dissected from early or late L3 larva in 50 µl PBS, pH 7.4. Dissected glands were fixed with 4% PFA PBS for 20 min at room temperature and permeabilized in PBST (PBS and 0.1% Triton X-100). Primary antibody incubation was performed overnight in PBST with 5% normal goat serum (Thermo Fisher Scientific). Secondary antibodies were diluted in PBST and incubated for 1 h at room temperature. Samples were mounted in 8 µl ProLong Diamond (Thermo Fisher Scientific) using self-adhesive reinforcement labels (Avery #32203) as spacers. Mounted samples were cured overnight at room temperature before sealing with nail polish. Primary antibodies were 1:1,000 rabbit anti-Lva (a gift from O. Papoulas and J. Sisson, The University of Texas at Austin, Austin, TX; Sisson et al., 2000); 1:30 mouse anti-Hrs (final concentration 3 µg/ml; Developmental Studies Hybridoma Bank; Riedel et al., 2016); 1:1,000 chicken anti-GFP (#ab13970, Abcam); and 1:100 rat anti-HA clone 3F10 (final concentration 1 µg/ml; Roche). Secondary antibodies conjugated to Alexa Fluor 405, 488, 568, and 647 were used at 1:500 (Thermo Fisher Scientific).

Image analysis

Cross-sectional areas of SGs were quantified using Volocity 6.3. Images were first deconvolved using the iterative restoration function with a confidence level of 99% and a maximum of 30 iterations. The find object function was used to identify and measure the surface area of SGs. Objects with a cross-sectional area <4 µm^2 were filtered out. Analyses were performed on three z-slices from a single acquisition (roughly one to three cells in the field of view) from three individual salivary glands.

Colocalization analyses were performed on original images using Volocity 6.3. Intensity threshold was chosen using the find object function to remove unwanted background signal. For each graph, five images from three independent experiments were used to calculate the average and standard deviation.

The percentage of SGs with P4M was quantified using Imaris 9.3.1 (Oxford Instruments). Original images were cropped into a smaller area encompassing mostly a single cell with three z-planes. Surfaces were rendered for SG and P4M from Sgs3-GFP and mCh-2xP4M signals with thresholding. Distance transformation was performed to measure the shortest distance for each of the SG surfaces to reach a P4M surface. Distances >0.5 µm represent SGs without nearby P4M surfaces surrounding them. The dynamics of GFP-PI4KII tubules was quantified by measuring the change in distance between frames using the manual tracking function from ImageJ (National Institutes of Health).

Statistical analysis

Raw data from ImageJ and Volocity 6.3 were imported into Microsoft Excel 2019. Student's *t* tests (two-tailed, unequal variance) were performed to test for statistical significance: **, P < 0.01; ***, P < 0.001; ****, P < 0.0001.

Box-and-whisker plots were generated using Microsoft Excel 2019. Each line of the box from bottom to top represents the 25th, 50th (median), and 75th percentile of the population. Bottom and top whiskers represent minimum and maximum values determined by 1.5× the interquartile range. Dots outside of the whiskers are samples considered statistical outliers.

Online supplemental materials

Table S1 shows the RNAi screen and CD63-GFP coexpression screen. Fig. S1 is a characterization of CD63 and Tsp29Fa in salivary gland cells. Fig. S2 shows CRISPR mutagenesis of *Tsp29Fa* and *Tsp29Fb*. Fig. S3 is a *PI4KIIΔ* characterization. Fig. S4 shows PI4KII and P4M analyses. Video 1 shows that GFP-PI4KII-positive tubules are more dynamic in *Pasl1$^{110\text{-}1}$* mutant.

Acknowledgments

We thank J. Brumell, U. Tepass, and members of the Brill laboratory for helpful discussions; M. Marks, H. Krämer, T. Balla, and U. Tepass for comments on the manuscript; A. Kiger, C. Wilson, M. Horowitz, Bloomington Drosophila Stock Center, and Vienna Drosophila RNAi Center for fly stocks; the Drosophila Genomics Resource Center for plasmids; O. Papoulas and the late J. Sisson for antibodies; and P. Paroutis and K. Lau (SickKids Imaging Facility) for assistance with microscopy and image analysis.

We acknowledge funding from the following sources: SickKids Restracomp Studentship, Canadian Institutes of Health Research Strategic Training Fellowship #TGF-53877, University of Toronto Open Fellowship, and Natural Sciences and Engineering Research Council of Canada Postgraduate Scholarships—Doctoral Program Studentship (to C-I.J. Ma); Lunenfeld Summer Studentship (to Y. Yang); Canadian Institutes of Health Research Operating Grants #PJT-162165 and #MOP-119483 and Canadian Institutes of Health Research Institute of Genetics #IG1-115714 (to J.A. Brill).

The authors declare no competing financial interests.

Author contributions: Conceptualization: C-I.J. Ma, J. Burgess, J.A. Brill; Data curation: C-I.J. Ma, J.A. Brill; Formal Analysis: C-I.J. Ma, Y. Yang; Funding acquisition: J.A. Brill; Investigation: C-I.J. Ma, Y. Yang, T. Kim, C.H. Chen, M. Vissa, J. Burgess; Methodology: C-I.J. Ma., G. Polevoy, J. Burgess, J.A. Brill; Project administration: J.A. Brill; Resources: C-I.J. Ma, Y. Yang, T. Kim, M. Vissa, G. Polevoy, J. Burgess, J.A. Brill;

Supervision: J.A. Brill; Validation: C-I.J. Ma, Y. Yang, T. Kim, C.H. Chen, M. Vissa, J. Burgess, J.A. Brill; Visualization: C-I.J. Ma, J.A. Brill; Writing – original draft: C-I.J. Ma, J.A. Brill; Writing – reviews & editing: C-I.J. Ma, Y. Yang, T. Kim, C.H. Chen, M. Vissa, J. Burgess, J.A. Brill.

Submitted: 2 August 2018
Revised: 30 November 2019
Accepted: 20 December 2019

References

Ailion, M., M. Hannemann, S. Dalton, A. Pappas, S. Watanabe, J. Hegermann, Q. Liu, H.-F. Han, M. Gu, M.Q. Goulding, et al. 2014. Two Rab2 interactors regulate dense-core vesicle maturation. *Neuron.* 82:167–180. https://doi.org/10.1016/j.neuron.2014.02.017

Asensio, C.S., D.W. Sirkis, J.W. Maas Jr., K. Egami, T.L. To, F.M. Brodsky, X. Shu, Y. Cheng, and R.H. Edwards. 2013. Self-assembly of VPS41 promotes sorting required for biogenesis of the regulated secretory pathway. *Dev. Cell.* 27:425–437. https://doi.org/10.1016/j.devcel.2013.10.007

Ashburner, M. 1989. Drosophila: A laboratory handbook. Cold Spring Harbor Laboratory Press, Cold Spring Harbor, NY.

Azouz, N.P., N. Zur, A. Efergan, N. Ohbayashi, M. Fukuda, D. Amihai, I. Hammel, M.E. Rothenberg, and R. Sagi-Eisenberg. 2014. Rab5 is a novel regulator of mast cell secretory granules: impact on size, cargo, and exocytosis. *J. Immunol.* 192:4043–4053. https://doi.org/10.4049/jimmunol.1302196

Bahl, K., S. Xie, G. Spagnol, P. Sorgen, N. Naslavsky, and S. Caplan. 2016. EHD3 Protein Is Required for Tubular Recycling Endosome Stabilization, and an Asparagine-Glutamic Acid Residue Pair within Its Eps15 Homology (EH) Domain Dictates Its Selective Binding to NPF Peptides. *J. Biol. Chem.* 291:13465–13478. https://doi.org/10.1074/jbc.M116.716407

Berditchevski, F., K.F. Tolias, K. Wong, C.L. Carpenter, and M.E. Hemler. 1997. A novel link between integrins, transmembrane-4 superfamily proteins (CD63 and CD81), and phosphatidylinositol 4-kinase. *J. Biol. Chem.* 272:2595–2598. https://doi.org/10.1074/jbc.272.5.2595

Biyasheva, A., T.-V. Do, Y. Lu, M. Vaskova, and A.J. Andres. 2001. Glue secretion in the Drosophila salivary gland: a model for steroid-regulated exocytosis. *Dev. Biol.* 231:234–251. https://doi.org/10.1006/dbio.2000.0126

Bonnemaison, M.L., B.A. Eipper, and R.E. Mains. 2013. Role of adaptor proteins in secretory granule biogenesis and maturation. *Front. Endocrinol. (Lausanne).* 4:101. https://doi.org/10.3389/fendo.2013.00101

Briguglio, J.S., S. Kumar, and A.P. Turkewitz. 2013. Lysosomal sorting receptors are essential for secretory granule biogenesis in Tetrahymena. *J. Cell Biol.* 203:537–550. https://doi.org/10.1083/jcb.201305086

Burgess, J., L.M. Del Bel, C.-I.J.C.J. Ma, B. Barylko, G. Polevoy, J. Rollins, J.P. Albanesi, H. Krämer, and J.A. Brill. 2012. Type II phosphatidylinositol 4-kinase regulates trafficking of secretory granule proteins in Drosophila. *Development.* 139:3040–3050. https://doi.org/10.1242/dev.077644

Burgess, J., M. Jauregui, J. Tan, J. Rollins, S. Lallet, P.A. Leventis, G.L. Boulianne, H.C. Chang, R. Le Borgne, H. Krämer, and J.A. Brill. 2011. AP-1 and clathrin are essential for secretory granule biogenesis in Drosophila. *Mol. Biol. Cell.* 22:2094–2105. https://doi.org/10.1091/mbc.e11-01-0054

Cai, B., S.S.P. Giridharan, J. Zhang, S. Saxena, K. Bahl, J.A. Schmidt, P.L. Sorgen, W. Guo, N. Naslavsky, and S. Caplan. 2013. Differential roles of C-terminal Eps15 homology domain proteins as vesiculators and tubulators of recycling endosomes. *J. Biol. Chem.* 288:30172–30180. https://doi.org/10.1074/jbc.M113.488627

Cattin-Ortolá, J., I. Topalidou, A. Dosey, A.J. Merz, and M. Ailion. 2017. The dense-core vesicle maturation protein CCCP-1 binds RAB-2 and membranes through its C-terminal domain. *Traffic.* 18:720–732. https://doi.org/10.1111/tra.12507

Christis, C., and S. Munro. 2012. The small G protein Arl1 directs the trans-Golgi-specific targeting of the Arf1 exchange factors BIG1 and BIG2. *J. Cell Biol.* 196:327–335. https://doi.org/10.1083/jcb.201107115

Corrigan, L., S. Redhai, A. Leiblich, S.-J. Fan, S.M.W. Perera, R. Patel, C. Gandy, S.M. Wainwright, J.F. Morris, F. Hamdy, et al. 2014. BMP-regulated exosomes from *Drosophila* male reproductive glands reprogram female behavior. *J. Cell Biol.* 206:671–688. https://doi.org/10.1083/jcb.201401072

Costantino, B.F.B., D.K. Bricker, K. Alexandre, K. Shen, J.R. Merriam, C. Antoniewski, J.L. Callender, V.C. Henrich, A. Presente, and A.J. Andres. 2008. A novel ecdysone receptor mediates steroid-regulated developmental events during the mid-third instar of Drosophila. *PLoS Genet.* 4:e1000102. https://doi.org/10.1371/journal.pgen.1000102

Csizmadia, T., P. Lőrincz, K. Hegedűs, S. Széplaki, P. Lőw, and G. Juhász. 2018. Molecular mechanisms of developmentally programmed crinophagy in *Drosophila*. *J. Cell Biol.* 217:361–374. https://doi.org/10.1083/jcb.201702145

D'Souza, R.S., R. Semus, E.A. Billings, C.B. Meyer, K. Conger, and J.E. Casanova. 2014. Rab4 orchestrates a small GTPase cascade for recruitment of adaptor proteins to early endosomes. *Curr. Biol.* 24:1187–1198. https://doi.org/10.1016/j.cub.2014.04.003

Del Vecchio, R.L., and P.F. Pilch. 1991. Phosphatidylinositol 4-kinase is a component of glucose transporter (GLUT 4)-containing vesicles. *J. Biol. Chem.* 266:13278–13283.

Duffield, A., E.J. Kamsteeg, A.N. Brown, P. Pagel, and M.J. Caplan. 2003. The tetraspanin CD63 enhances the internalization of the H,K-ATPase β-subunit. *Proc. Natl. Acad. Sci. USA.* 100:15560–15565. https://doi.org/10.1073/pnas.2536699100

Edwards, S.L., N.K. Charlie, J.E. Richmond, J. Hegermann, S. Eimer, and K.G. Miller. 2009. Impaired dense core vesicle maturation in *Caenorhabditis elegans* mutants lacking Rab2. *J. Cell Biol.* 186:881–895. https://doi.org/10.1083/jcb.200902095

Farkaš, R., and G. Šutáková. 1998. Ultrastructural changes of Drosophila larval and prepupal salivary glands cultured in vitro with ecdysone. *In Vitro Cell. Dev. Biol. Anim.* 34:813–823. https://doi.org/10.1007/s11626-998-0036-7

Geisert, E.E. Jr., R.W. Williams, G.R. Geisert, L. Fan, A.M. Asbury, H.T. Maecker, J. Deng, and S. Levy. 2002. Increased brain size and glial cell number in CD81-null mice. *J. Comp. Neurol.* 453:22–32. https://doi.org/10.1002/cne.10364

Gillooly, D.J., I.C. Morrow, M. Lindsay, R. Gould, N.J. Bryant, J.M. Gaullier, R.G. Parton, and H. Stenmark. 2000. Localization of phosphatidylinositol 3-phosphate in yeast and mammalian cells. *EMBO J.* 19:4577–4588. https://doi.org/10.1093/emboj/19.17.4577

Goldstein, L.S.B., and E.A. Fyrberg. 1994. Drosophila melanogaster : practical uses in cell and molecular biology. Academic Press, Cambridge, MA.

Grabner, C.P., S.D. Price, A. Lysakowski, A.L. Cahill, and A.P. Fox. 2006. Regulation of large dense-core vesicle volume and neurotransmitter content mediated by adaptor protein 3. *Proc. Natl. Acad. Sci. USA.* 103:10035–10040. https://doi.org/10.1073/pnas.0509844103

Gramates, L.S., S.J. Marygold, G.D. Santos, J.-M. Urbano, G. Antonazzo, B.B. Matthews, A.J. Rey, C.J. Tabone, M.A. Crosby, D.B. Emmert, et al. the FlyBase Consortium. 2017. FlyBase at 25: looking to the future. *Nucleic Acids Res.* 45(D1):D663–D671. https://doi.org/10.1093/nar/gkw1016

Guo, J., M.R. Wenk, L. Pellegrini, F. Onofri, F. Benfenati, and P. De Camilli. 2003. Phosphatidylinositol 4-kinase type IIalpha is responsible for the phosphatidylinositol 4-kinase activity associated with synaptic vesicles. *Proc. Natl. Acad. Sci. USA.* 100:3995–4000. https://doi.org/10.1073/pnas.0230488100

Hammond, G.R.V., M.P. Machner, and T. Balla. 2014. A novel probe for phosphatidylinositol 4-phosphate reveals multiple pools beyond the Golgi. *J. Cell Biol.* 205:113–126. https://doi.org/10.1083/jcb.201312072

Harrison-Lavoie, K.J., G. Michaux, L. Hewlett, J. Kaur, M.J. Hannah, W.W.Y. Lui-Roberts, K.E. Norman, and D.F. Cutler. 2006. P-selectin and CD63 use different mechanisms for delivery to Weibel-Palade bodies. *Traffic.* 7:647–662. https://doi.org/10.1111/j.1600-0854.2006.00415.x

Hatskelzon, L., B.I. Dalal, A. Shalev, C. Robertson, and J.M. Gerrard. 1993. Wide distribution of granulophysin epitopes in granules of human tissues. *Lab. Invest.* 68:509–519.

Jean, S., S. Cox, E.J. Schmidt, F.L. Robinson, and A. Kiger. 2012. Sbf/MTMR13 coordinates PI(3)P and Rab21 regulation in endocytic control of cellular remodeling. *Mol. Biol. Cell.* 23:2723–2740. https://doi.org/10.1091/mbc.e12-05-0375

Jović, M., F. Kieken, N. Naslavsky, P.L. Sorgen, and S. Caplan. 2009. Eps15 homology domain 1-associated tubules contain phosphatidylinositol-4-phosphate and phosphatidylinositol-(4,5)-bisphosphate and are required for efficient recycling. *Mol. Biol. Cell.* 20:2731–2743. https://doi.org/10.1091/mbc.e08-11-1102

Juhász, G., J.H. Hill, Y. Yan, M. Sass, E.H. Baehrecke, J.M. Backer, and T.P. Neufeld. 2008. The class III PI(3)K Vps34 promotes autophagy and endocytosis but not TOR signaling in Drosophila. *J. Cell Biol.* 181:655–666. https://doi.org/10.1083/jcb.200712051

Jung, G., J. Wang, P. Wlodarski, B. Barylko, D.D. Binns, H. Shu, H.L. Yin, and J.P. Albanesi. 2008. Molecular determinants of activation and

membrane targeting of phosphoinositol 4-kinase IIbeta. *Biochem. J.* 409: 501–509. https://doi.org/10.1042/BJ20070821

Klein, O., A. Roded, N. Zur, N.P. Azouz, O. Pasternak, K. Hirschberg, I. Hammel, P.A. Roche, A. Yatsu, M. Fukuda, et al. 2017. Rab5 is critical for SNAP23 regulated granule-granule fusion during compound exocytosis. *Sci. Rep.* 7:15315. https://doi.org/10.1038/s41598-017-15047-8

Knobeloch, K.P., M.D. Wright, A.F. Ochsenbein, O. Liesenfeld, J. Löhler, R.M. Zinkernagel, I. Horak, and Z. Orinska. 2000. Targeted inactivation of the tetraspanin CD37 impairs T-cell-dependent B-cell response under suboptimal costimulatory conditions. *Mol. Cell. Biol.* 20:5363–5369. https://doi.org/10.1128/MCB.20.15.5363-5369.2000

Koles, K., E.M. Messelaar, Z. Feiger, C.J. Yu, C.A. Frank, and A.A. Rodal. 2015. The EHD protein Past1 controls postsynaptic membrane elaboration and synaptic function. *Mol. Biol. Cell.* 26:3275–3288. https://doi.org/10.1091/mbc.e15-02-0093

Kontur, C., S. Kumar, X. Lan, J.K. Pritchard, and A.P. Turkewitz. 2016. Whole Genome Sequencing Identifies a Novel Factor Required for Secretory Granule Maturation in Tetrahymena thermophila. *G3 (Bethesda).* 6: 2505–2516. https://doi.org/10.1534/g3.116.028878

Kristiansen, S., T. Ramlal, and A. Klip. 1998. Phosphatidylinositol 4-kinase, but not phosphatidylinositol 3-kinase, is present in GLUT4-containing vesicles isolated from rat skeletal muscle. *Biochem. J.* 335:351–356. https://doi.org/10.1042/bj3350351

Lui-Roberts, W.W.Y., L.M. Collinson, L.J. Hewlett, G. Michaux, and D.F. Cutler. 2005. An AP-1/clathrin coat plays a novel and essential role in forming the Weibel-Palade bodies of endothelial cells. *J. Cell Biol.* 170: 627–636. https://doi.org/10.1083/jcb.200503054

Maecker, H.T., and S. Levy. 1997. Normal lymphocyte development but delayed humoral immune response in CD81-null mice. *J. Exp. Med.* 185: 1505–1510. https://doi.org/10.1084/jem.185.8.1505

Marks, M.S., H.F. Heijnen, and G. Raposo. 2013. Lysosome-related organelles: unusual compartments become mainstream. *Curr. Opin. Cell Biol.* 25: 495–505. https://doi.org/10.1016/j.ceb.2013.04.008

Marois, E., A. Mahmoud, and S. Eaton. 2006. The endocytic pathway and formation of the Wingless morphogen gradient. *Development.* 133: 307–317. https://doi.org/10.1242/dev.02197

McKenzie, J.E., B. Raisley, X. Zhou, N. Naslavsky, T. Taguchi, S. Caplan, and D. Sheff. 2012. Retromer guides STxB and CD8-M6PR from early to recycling endosomes, EHD1 guides STxB from recycling endosome to Golgi. *Traffic.* 13:1140–1159. https://doi.org/10.1111/j.1600-0854.2012.01374.x

Messenger, S.W., D.D.H. Thomas, M.A. Falkowski, J.A. Byrne, F.S. Gorelick, and G.E. Groblewski. 2013. Tumor protein D52 controls trafficking of an apical endolysosomal secretory pathway in pancreatic acinar cells. *Am. J. Physiol. Gastrointest. Liver Physiol.* 305:G439–G452. https://doi.org/10.1152/ajpgi.00143.2013

Mills, I.G., G.J.K. Praefcke, Y. Vallis, B.J. Peter, L.E. Olesen, J.L. Gallop, P.J.G. Butler, P.R. Evans, and H.T. McMahon. 2003. EpsinR: an AP1/clathrin interacting protein involved in vesicle trafficking. *J. Cell Biol.* 160: 213–222. https://doi.org/10.1083/jcb.200208023

Miyazaki, T., U. Müller, and K.S. Campbell. 1997. Normal development but differentially altered proliferative responses of lymphocytes in mice lacking CD81. *EMBO J.* 16:4217–4225. https://doi.org/10.1093/emboj/16.14.4217

Mizuno, K., T. Tolmachova, D.S. Ushakov, M. Romao, M. Åbrink, M.A. Ferenczi, G. Raposo, and M.C. Seabra. 2007. Rab27b regulates mast cell granule dynamics and secretion. *Traffic.* 8:883–892. https://doi.org/10.1111/j.1600-0854.2007.00571.x

Morelli, E., P. Ginefra, V. Mastrodonato, G.V. Beznoussenko, T.E. Rusten, D. Bilder, H. Stenmark, A.A. Mironov, and T. Vaccari. 2014. Multiple functions of the SNARE protein Snap29 in autophagy, endocytic, and exocytic trafficking during epithelial formation in *Drosophila*. *Autophagy.* 10:2251–2268. https://doi.org/10.4161/15548627.2014.981913

Nishibori, M., B. Cham, A. McNicol, A. Shalev, N. Jain, and J.M. Gerrard. 1993. The protein CD63 is in platelet dense granules, is deficient in a patient with Hermansky-Pudlak syndrome, and appears identical to granulophysin. *J. Clin. Invest.* 91:1775–1782. https://doi.org/10.1172/JCI116388

Olswang-Kutz, Y., Y. Gertel, S. Benjamin, O. Sela, O. Pekar, E. Arama, H. Steller, M. Horowitz, and D. Segal. 2009. Drosophila Past1 is involved in endocytosis and is required for germline development and survival of the adult fly. *J. Cell Sci.* 122:471–480. https://doi.org/10.1242/jcs.038521

Panáková, D., H. Sprong, E. Marois, C. Thiele, and S. Eaton. 2005. Lipoprotein particles are required for Hedgehog and Wingless signalling. *Nature.* 435:58–65. https://doi.org/10.1038/nature03504

Panaretou, C., and S.A. Tooze. 2002. Regulation and recruitment of phosphatidylinositol 4-kinase on immature secretory granules is independent of ADP-ribosylation factor 1. *Biochem. J.* 363:289–295. https://doi.org/10.1042/bj3630289

Perez-Hernandez, D., C. Gutiérrez-Vázquez, I. Jorge, S. López-Martín, A. Ursa, F. Sánchez-Madrid, J. Vázquez, and M. Yáñez-Mó. 2013. The intracellular interactome of tetraspanin-enriched microdomains reveals their function as sorting machineries toward exosomes. *J. Biol. Chem.* 288:11649–11661. https://doi.org/10.1074/jbc.M112.445304

Polevoy, G., H.C. Wei, R. Wong, Z. Szentpetery, Y.J. Kim, P. Goldbach, S.K. Steinbach, T. Balla, and J.A. Brill. 2009. Dual roles for the Drosophila PI 4-kinase Four wheel drive in localizing Rab11 during cytokinesis. *J. Cell Biol.* 187:847–858. https://doi.org/10.1083/jcb.200908107

Pols, M.S., and J. Klumperman. 2009. Trafficking and function of the tetraspanin CD63. *Exp. Cell Res.* 315:1584–1592. https://doi.org/10.1016/j.yexcr.2008.09.020

Ponton, F., M.-P.P. Chapuis, M. Pernice, G.A. Sword, and S.J. Simpson. 2011. Evaluation of potential reference genes for reverse transcription-qPCR studies of physiological responses in Drosophila melanogaster. *J. Insect Physiol.* 57:840–850. https://doi.org/10.1016/j.jinsphys.2011.03.014

Raposo, G., M.S. Marks, and D.F. Cutler. 2007. Lysosome-related organelles: driving post-Golgi compartments into specialisation. *Curr. Opin. Cell Biol.* 19:394–401. https://doi.org/10.1016/j.ceb.2007.05.001

Redhai, S., J.E.E.U. Hellberg, M. Wainwright, S.W. Perera, F. Castellanos, B. Kroeger, C. Gandy, A. Leiblich, L. Corrigan, T. Hilton, et al. 2016. Regulation of Dense-Core Granule Replenishment by Autocrine BMP Signalling in Drosophila Secondary Cells. *PLoS Genet.* 12:e1006366. https://doi.org/10.1371/journal.pgen.1006366

Riedel, F., A.K. Gillingham, C. Rosa-Ferreira, A. Galindo, and S. Munro. 2016. An antibody toolkit for the study of membrane traffic in Drosophila melanogaster. *Biol. Open.* 5:987–992. https://doi.org/10.1242/bio.018937

Sasidharan, N., M. Sumakovic, M. Hannemann, J. Hegermann, J.F. Liewald, C. Olendrowitz, S. Koenig, B.D. Grant, S.O. Rizzoli, A. Gottschalk, and S. Eimer. 2012. RAB-5 and RAB-10 cooperate to regulate neuropeptide release in Caenorhabditis elegans. *Proc. Natl. Acad. Sci. USA.* 109: 18944–18949. https://doi.org/10.1073/pnas.1203306109

Schulze, U., S. Brast, A. Grabner, C. Albiker, B. Snieder, S. Holle, E. Schlatter, R. Schröter, H. Pavenstädt, E. Herrmann, et al. 2017. Tetraspanin CD63 controls basolateral sorting of organic cation transporter 2 in renal proximal tubules. *FASEB J.* 31:1421–1433. https://doi.org/10.1096/fj.201600901R

Sharma, M., M. Jovic, F. Kieken, N. Naslavsky, P. Sorgen, and S. Caplan. 2009. A model for the role of EHD1-containing membrane tubules in endocytic recycling. *Commun. Integr. Biol.* 2:431–433. https://doi.org/10.4161/cib.2.5.9157

Sisson, J.C., C. Field, R. Ventura, A. Royou, and W. Sullivan. 2000. Lava lamp, a novel peripheral golgi protein, is required for Drosophila melanogaster cellularization. *J. Cell Biol.* 151:905–918. https://doi.org/10.1083/jcb.151.4.905

Sparvoli, D., E. Richardson, H. Osakada, X. Lan, M. Iwamoto, G.R. Bowman, C. Kontur, W.A. Bourland, D.H. Lynn, J.K. Pritchard, et al. 2018. Remodeling the Specificity of an Endosomal CORVET Tether Underlies Formation of Regulated Secretory Vesicles in the Ciliate Tetrahymena thermophila. *Curr. Biol.* 28:697–710.e13. https://doi.org/10.1016/j.cub.2018.01.047

Tan, J., and J.A. Brill. 2014. Cinderella story: PI4P goes from precursor to key signaling molecule. *Crit. Rev. Biochem. Mol. Biol.* 49:33–58. https://doi.org/10.3109/10409238.2013.853024

Tan, J., K. Oh, J. Burgess, D.R. Hipfner, and J.A. Brill. 2014. PI4KIIIα is required for cortical integrity and cell polarity during Drosophila oogenesis. *J. Cell Sci.* 127:954–966. https://doi.org/10.1242/jcs.129031

Tarrant, J.M., J. Groom, D. Metcalf, R. Li, B. Borobokas, M.D. Wright, D. Tarlinton, and L. Robb. 2002. The absence of Tssc6, a member of the tetraspanin superfamily, does not affect lymphoid development but enhances in vitro T-cell proliferative responses. *Mol. Cell. Biol.* 22: 5006–5018. https://doi.org/10.1128/MCB.22.14.5006-5018.2002

Topalidou, I., J. Cattin-Ortolá, A.L. Pappas, K. Cooper, G.E. Merrihew, M.J. MacCoss, and M. Ailion. 2016. The EARP Complex and Its Interactor EIPR-1 Are Required for Cargo Sorting to Dense-Core Vesicles. *PLoS Genet.* 12:e1006074. https://doi.org/10.1371/journal.pgen.1006074

Torres, I.L., C. Rosa-Ferreira, and S. Munro. 2014. The Arf family G protein Arl1 is required for secretory granule biogenesis in *Drosophila*. *J. Cell Sci.* 127:2151–2160. https://doi.org/10.1242/jcs.122028

Tsai, J.W., R. Kostyleva, P.L. Chen, I.M. Rivas-Serna, M.T. Clandinin, I.A. Meinertzhagen, and T.R. Clandinin. 2019. Transcriptional Feedback Links Lipid Synthesis to Synaptic Vesicle Pools in Drosophila Photoreceptors. *Neuron.* 101:721–737.e4. https://doi.org/10.1016/j.neuron.2019.01.015

van Niel, G., S. Charrin, S. Simoes, M. Romao, L. Rochin, P. Saftig, M.S. Marks, E. Rubinstein, and G. Raposo. 2011. The tetraspanin CD63 regulates ESCRT-independent and -dependent endosomal sorting during melanogenesis. *Dev. Cell.* 21:708–721. https://doi.org/10.1016/j.devcel.2011.08.019

Verweij, F.J., M.A.J. van Eijndhoven, E.S. Hopmans, T. Vendrig, T. Wurdinger, E. Cahir-McFarland, E. Kieff, D. Geerts, R. van der Kant, J. Neefjes, et al. 2011. LMP1 association with CD63 in endosomes and secretion via exosomes limits constitutive NF-κB activation. *EMBO J.* 30: 2115–2129. https://doi.org/10.1038/emboj.2011.123

Wang, J., H.Q. Sun, E. Macia, T. Kirchhausen, H. Watson, J.S. Bonifacino, and H.L. Yin. 2007. PI4P promotes the recruitment of the GGA adaptor proteins to the trans-Golgi network and regulates their recognition of the ubiquitin sorting signal. *Mol. Biol. Cell.* 18:2646–2655. https://doi.org/10.1091/mbc.e06-10-0897

Wang, Y.J., J. Wang, H.Q. Sun, M. Martinez, Y.X. Sun, E. Macia, T. Kirchhausen, J.P. Albanesi, M.G. Roth, and H.L. Yin. 2003. Phosphatidylinositol 4 phosphate regulates targeting of clathrin adaptor AP-1 complexes to the Golgi. *Cell.* 114:299–310. https://doi.org/10.1016/S0092-8674(03)00603-2

Xu, H., G.L. Boulianne, and W.S. Trimble. 2002. Drosophila syntaxin 16 is a Q-SNARE implicated in Golgi dynamics. *J. Cell Sci.* 115:4447–4455. https://doi.org/10.1242/jcs.00139

Xu, Z., G. Huang, and K.V. Kandror. 2006. Phosphatidylinositol 4-kinase type IIalpha is targeted specifically to cellugyrin-positive glucose transporter 4 vesicles. *Mol. Endocrinol.* 20:2890–2897. https://doi.org/10.1210/me.2006-0193

Yauch, R.L., and M.E. Hemler. 2000. Specific interactions among transmembrane 4 superfamily (TM4SF) proteins and phosphoinositide 4-kinase. *Biochem. J.* 351:629–637. https://doi.org/10.1042/bj3510629

Yu, M., S. Yang, H. Sun, and Q. Xia. 2016. CD63 Promotes Hemocyte-Mediated Phagocytosis in the Clam, *Paphia undulata*. *J. Immunol. Res.* 2016:7893490. https://doi.org/10.1155/2016/7893490

Supplemental material

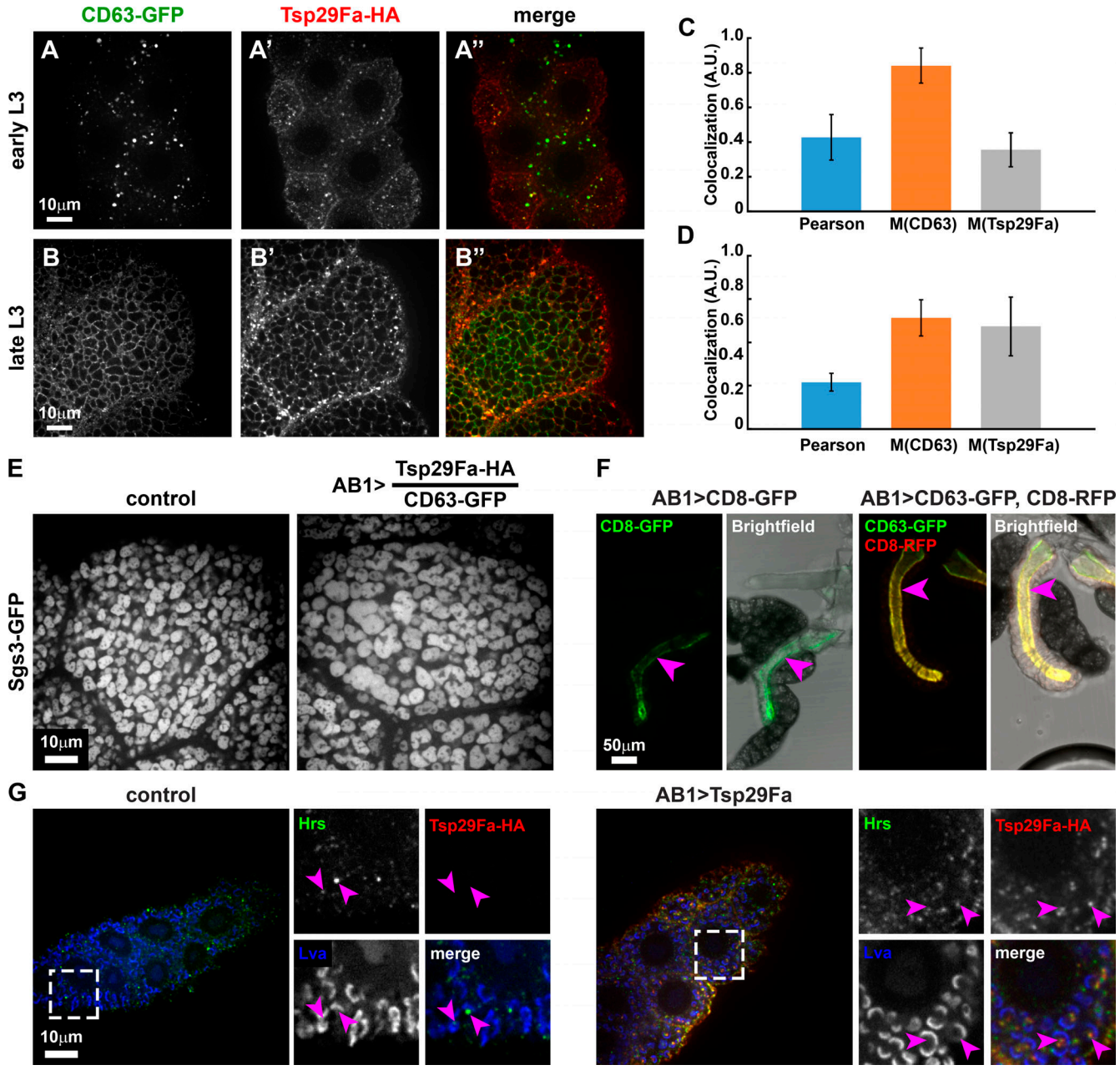

Figure S1. **Characterization of CD63 and Tsp29Fa in salivary gland cells. (A, B, and E–G)** Spinning-disc confocal images of L3 salivary gland cells. **(A and B)** Cells from early (A) and late (B) L3 expressing CD63-GFP and Tsp29Fa-Flag-HA driven by one copy of AB1-GAL4, fixed and stained for GFP (green) and HA (red). **(C and D)** Colocalization analysis of CD63-GFP and Tsp29Fa-Flag-HA from early (C) and late (D) L3 salivary gland cells. Error bars indicate standard deviation. **(C)** Pearson's = 0.43 ± 0.13, M(CD63) = 0.84 ± 0.10, M(Tsp29Fa) = 0.36 ± 0.10. **(D)** Pearson's = 0.22 ± 0.041, M(CD63) = 0.51 ± 0.084, M(Tsp29Fa) = 0.47 ± 0.14. Analysis was performed on a total of five images from two independent experiments. **(E)** Live cells expressing Sgs3-GFP (grayscale) in control cell (left) or cell with one copy of Tsp29-Flag-HA and one copy of CD63-GFP driven by two copies of AB1-Gal4 driver (right). **(F)** Live salivary gland cells expressing CD8-GFP (left) or CD63-GFP and CD8-RFP (right) with AB1-Gal4 driver. Magenta arrows indicate apical membranes in confocal and corresponding merged fluorescence and bright-field images. **(G)** Salivary gland cells without (left) or with (right) one copy of Tsp29Fa-Flag-HA driven by AB1-Gal4. Cells were fixed and stained for Hrs (green, EE), Lva (blue, cis-Golgi), and HA (red, Tsp29Fa-Flag-HA). Dashed boxes mark regions magnified 2.5-fold in insets. Magenta arrows show EE adjacent to cup-shaped cis-Golgi structures.

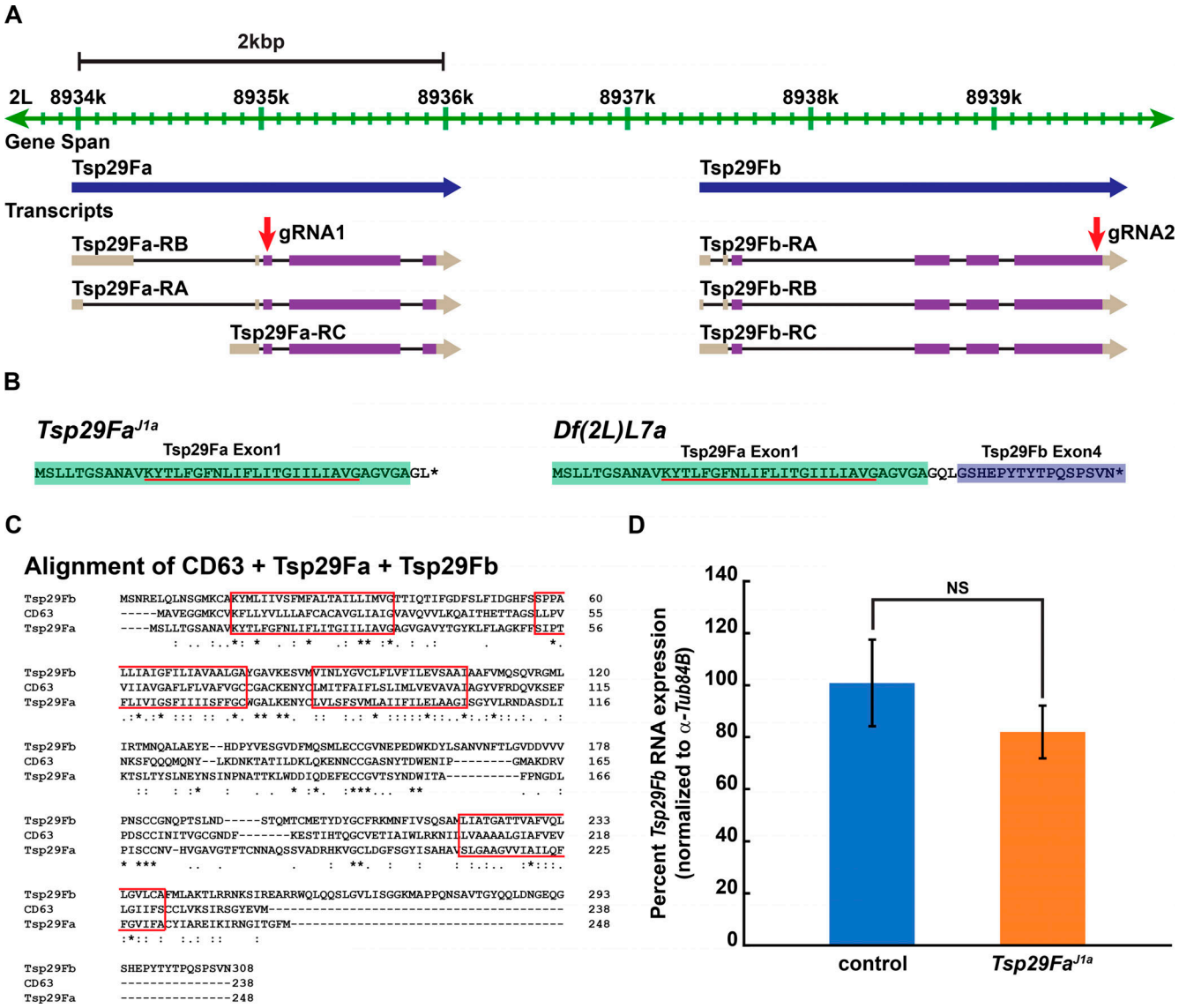

Figure S2. **CRISPR mutagenesis of *Tsp29Fa* and *Tsp29Fb*. (A)** Genomic region encoding *Tsp29Fa* and *Tsp29Fb* on chromosome 2L (green line). Blue arrows indicate span and direction of *Tsp29Fa* and *Tsp29Fb* genes. Each gene has three predicted transcripts (denoted RA, RB, and RC), where beige boxes represent noncoding and purple boxes represent coding regions of exons (adapted from Flybase, release 6.20). Red arrows point to locations where guide RNAs gRNA1 and gRNA2 were targeted for CRISPR-Cas9 gene editing. **(B)** Predicted amino acid sequences encoded by *Tsp29*^{J1a} (left) and *Df(2L)L7a* (right) deletions. Green indicates unaltered Tsp29Fa amino acid sequences and purple indicates unaltered Tsp29Fb amino acid sequence. *, stop codon. Red underline marks transmembrane domain. **(C)** ClustalW alignment of mouse CD63 with *Drosophila* Tsp29Fa and Tsp29FB. Red boxes indicate the four conserved transmembrane domains, based on predictions from UniprotKB for mouse CD63. **(D)** Bar graph showing qRT-PCR analysis of *Tsp29Fb* mRNA levels in control and *Tsp29Fa*^{J1a} L3 larvae normalized to *Δ-tubulin84B* mRNA. *n* = 3 independent experiments. Error bars indicate standard deviation.

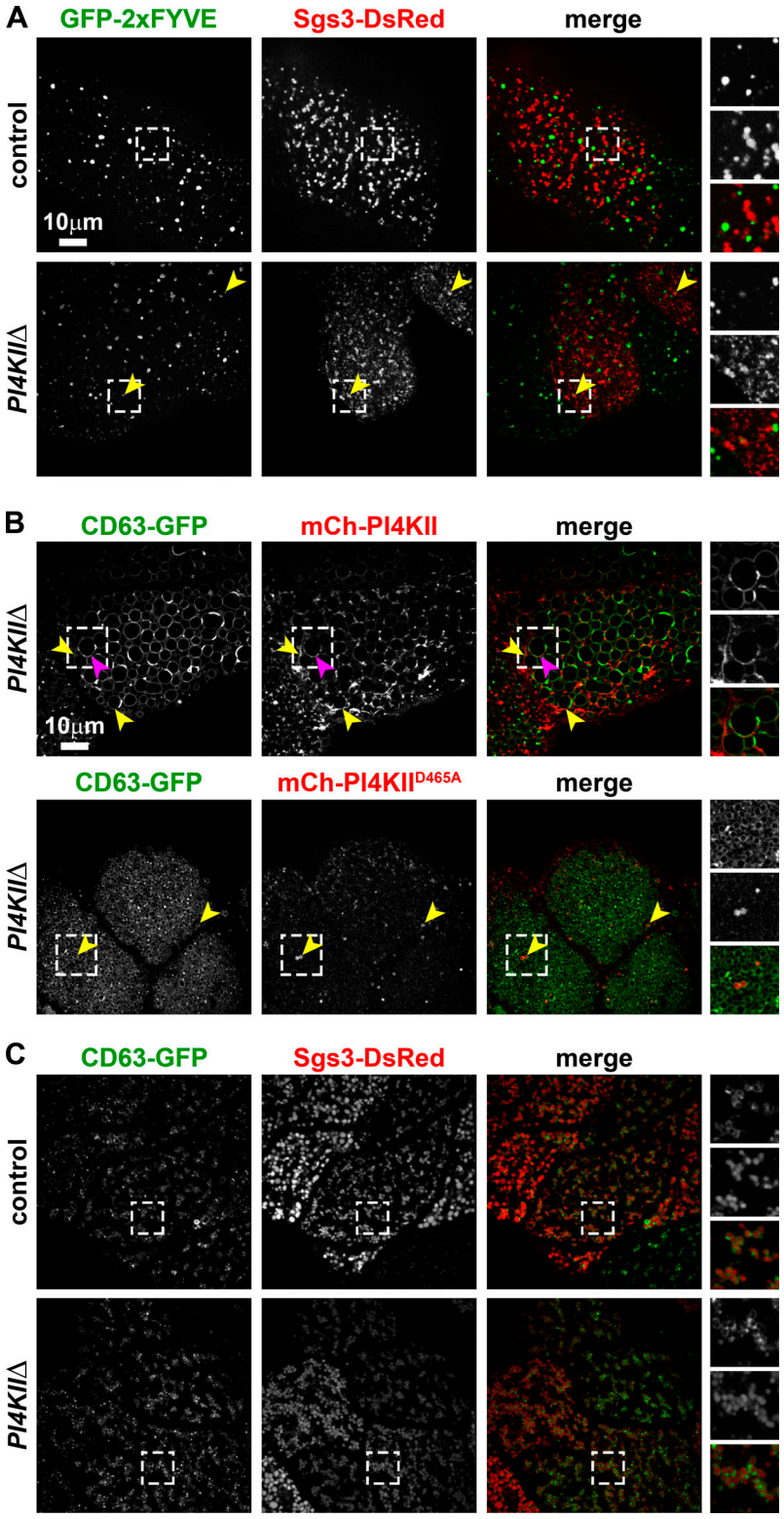

Figure S3. ***PI4KIIΔ* characterization. (A–C)** Spinning-disc confocal images of live early (A and C) or late (B) L3 salivary gland cells. **(A)** Early L3 cells expressing GFP-2xFYVE (green) and Sgs3-DsRed (red) in control (top) or *PI4KIIΔ* mutants (bottom). Colocalization of GFP-2xFYVE and Sgs3-DsRed is marked by yellow arrowheads. Dashed boxes mark regions that are magnified 2.1-fold in the insets. **(B)** Top: *PI4KIIΔ* cells expressing CD63-GFP (green) with kinase active mCh-PI4KII (red). Yellow arrowheads mark mCh-PI4KII tubules forming contacts with CD63-GFP–positive SG membranes. Magenta arrowhead marks colocalization of CD63-GFP and mCh-PI4KII on SG membranes. Dashed boxes mark regions that are magnified 1.6-fold in the insets. Bottom: *PI4KIIΔ* cells expressing CD63-GFP (green) with kinase-dead mCh-PI4KII^{CAT} (red). Yellow arrowheads mark mCh-PI4KII^{CAT} within the lumen of CD63-GFP vesicles. Dashed boxes mark regions magnified 2.1-fold in the insets. **(C)** Early L3 cells expressing CD63-GFP (green) and Sgs3-DsRed (red) in control (top) or *PI4KIIΔ* mutants (bottom). Dashed boxes mark regions that are magnified 2.1-fold in the insets.

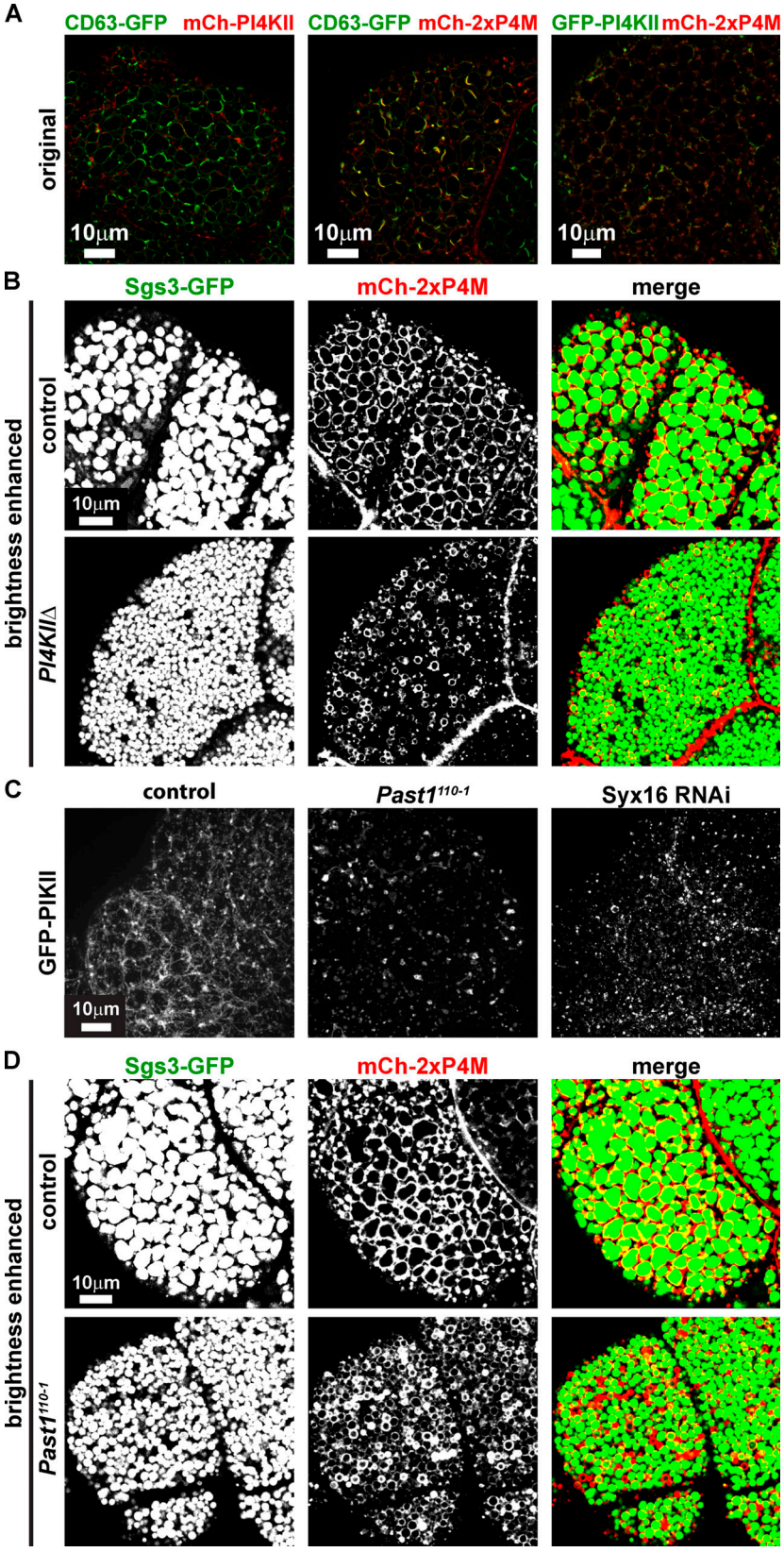

Figure S4. **PI4KII and P4M analyses. (A, B, and D)** Leica point-scanning confocal images of live late L3 salivary gland cells. **(A)** Original images without Lightning processing of Fig. 6 A′′ (left), Fig. 6 C′′ (middle), Fig. 6 E′′(right). **(B)** Brightness-enhanced images of Fig 6, G–G′′ (top row) and Fig 6, H–H′′ (bottom row). **(C)** Projections of 30 spinning-disc confocal planes of live late L3 salivary gland cells expressing GFP-PI4KII (grayscale) in control (left), *Past1*$^{110-1}$ mutant (middle), or *Syx16* RNAi (right). Corresponding to Fig. 7, A–C. **(D)** Brightness-enhanced images of Fig 7, G–G′′ (top row) and Fig 7, H–H′′ (bottom row). B and D were enhanced for brightness to reveal whether 2xP4M localized to immature SGs at a low level.

Video 1. **GFP-PI4KII-positive tubules are more dynamic in *Past1*$^{110\text{-}1}$ mutant.** Time-lapse video of spinning-disc confocal images of live L3 salivary gland cells expressing GFP-PI4KII in control (left) or *Past1*$^{110\text{-}1}$ mutant (right). Images were acquired every 300 ms for 30 s, time stamp is minutes:seconds. Frame rate is 13 frames/s. Corresponds to Fig. 7, D and E.

One table is provided online. Table S1 shows the RNAi screen and CD63-GFP coexpression screen.